

## Chapter 15

# Assessing the Role of Tectono-Magmatic Setting in the Precious Metal (Au, Ag, PGE) and Critical Metal (Te, Se, Bi) Endowment of Porphyry Cu Deposits

Katie McFall,<sup>1</sup> Iain McDonald,<sup>1</sup> and Jamie J. Wilkinson<sup>2,3</sup>

<sup>1</sup>Cardiff University School of Earth and Ocean Sciences, Main Building, Park Place, Cardiff CF10 3AT, United Kingdom

<sup>2</sup>LODE, Department of Earth Sciences, Natural History Museum, Cromwell Road, London SW7 5BD, United Kingdom

<sup>3</sup>Department of Earth Science and Engineering, Imperial College London, Exhibition Road, London SW7 2AZ, United Kingdom

### Abstract

Porphyry Cu deposits commonly contain critical and precious metal by-products, including the chalcophile and siderophile elements, Au, Pd, Pt, Ag, Te, Se, and Bi. These elements partition into residual sulfides during the partial melting of mantle wedge peridotite during subduction, potentially depleting the source magma for subduction-related porphyry Cu deposits. The chalcophile-rich residual sulfides in subduction-modified subcontinental lithosphere are thought to be the source of metals in postsubduction porphyry Cu deposits, and as such these deposits may be more enriched in chalcophile and siderophile elements than subduction-related porphyry deposits, although many postsubduction deposits have low Au grades. We test this by presenting whole-rock assay and PGE data with in situ LA-ICP-MS trace element data from sulfide minerals from three porphyry Cu deposits. The Skouries Cu-Au-(PGE) porphyry deposit, Greece, and the Muratdere Cu-Au-Mo porphyry deposit, Turkey are both postsubduction; these are contrasted with the El Teniente Cu-Mo porphyry deposit, Chile, which is a classic subduction-related system. By comparing these results with a newly compiled global dataset of trace element concentrations in sulfides from 18 other porphyry Cu deposits we show that postsubduction porphyry Cu deposit sulfides are relatively enriched in Bi, Sb, Te, and Se compared to sulfide minerals from subduction-related deposits. However, although some critical and precious metals (Ag, Bi, and Se) mainly reside in primary sulfide ore minerals, others (Au, Te, Pd, and Pt) are predominantly hosted in minor accessory minerals. Whole-rock data from mineralized samples show that although the Skouries and Muratdere deposits are enriched in Au compared with El Teniente, globally both subduction-related and postsubduction deposits can be precious and critical metal enriched, with metal endowment independent of tectonic setting. PGE-enriched porphyry Cu deposits are also enriched in Bi, Te, and Au, and semimetal melts are suggested to play an important role in PGE transport and concentration in porphyry Cu deposits.

### Introduction

Porphyry Cu deposits supply a large proportion of the world's Cu, and Mo (Sinclair, 2007; Sillitoe, 2010). They also contain many valuable potential by-products, including precious metals (Au, Ag, and PGE) and critical metals (Te, Se, and Bi), elements which are essential for green technologies but for which there is a supply risk. Tellurium and Se, for example, are essential for solar panel manufacture and are currently almost exclusively sourced from anode slimes from Cu production, much of which is from porphyry deposits (Gunn, 2014). Porphyry deposits can also contain significant amounts of Bi, which is primarily used in pharmaceuticals but also has applications in superconductors, thermo-electric power generation, and as a substitute for lead. Platinum group elements (PGE) are also present in elevated concentrations (>1 ppm) in some porphyry systems (Tarkian and Stribrny, 1999); these are used in catalytic converters and hydrogen fuel cell technology, with applications in electric car production. In order to exploit these potential by-products, however, we need to

understand their geometallurgy and the controls on their endowment to allow more efficient extraction and exploration.

The controls on metal endowments in porphyry copper deposits are still unclear. For example, porphyry copper deposits form in different tectono-magmatic settings and this may affect the endowment of critical and precious metals, particularly the chalcophile (here defined as sulfide-loving) and siderophile elements Au, Te, Se, Bi, Ag, and PGE (e.g., Richards, 2009; Holwell et al., 2019). The majority of porphyry deposits are in active continental margin settings (Liégeois et al., 1998; Richards, 2009), forming above active subduction zones in association with arc volcanism (e.g., Sillitoe, 1973). However, they can also form in postsubduction settings, through slab break off, lithospheric delamination, and asthenospheric upwelling during extension (Richards, 2009). Richards (2009) proposed that these “postsubduction” porphyries should be more enriched in Au than classic, arc-associated deposits.

Subduction-related deposits derive their metal and volatile contents from the dehydrating subducting slab, the partial melting of the metasomatized mantle wedge, and processes operating in the deep crust, such as assimilation. Copper, Ag, Au, and PGE are thought to be mainly sourced from the

<sup>1</sup>Corresponding author: e-mail address, k.mcfall@ucl.ac.uk

metasomatized mantle wedge (McInnes et al., 1999; Jenner, 2017), whereas Bi is more hydrothermally mobile and may be derived from hydrothermal sulfides in the upper oceanic crust of the downgoing slab (e.g., Ringwood, 1977; Sillitoe, 2010; Jenner, 2017). Tellurium is present in mantle sulfides (Hattori et al., 2002) but is also present in high concentrations in sea-floor sediments, particularly ferromanganese crusts and nodules (e.g., Hein et al., 2003; Lusty et al., 2018); consequently, it is likely sourced from a combination of both the slab and mantle wedge.

Most arc magmas are likely to reach sulfide saturation on ascent (Matjuschkin et al., 2016) and form residual sulfides which, due to their relatively low abundance, will have a very high R number ( $R = \text{mass of silicate melt}/\text{mass of sulfide}$ ; Campbell and Naldrett, 1979). The metal content of these sulfides is determined by a combination of the sulfide R number, the metal content of the silicate melt, and the distribution coefficient of the metal between sulfide (liquid or solid) and silicate melts ( $D^{\text{sul/sil}}$ ; Campbell and Naldrett, 1979). Chalcophile and siderophile elements have  $D^{\text{sul/sil}}$  in the order  $\text{PGE} > \text{Au} > \text{Te} > \text{Ag} > \text{Cu} > \text{Ni} > \text{Se} > \text{Bi} > \text{Co}$  (Patten et al., 2013; Mungall and Brenan, 2014) so that PGE and Au are particularly susceptible to extraction by sulfide formation. This means that, although volumetrically minor, these sulfides have the potential to extract most of the PGE and Au, along with Te, and some Cu, Ag, Se, and Bi from the silicate melt. If these sulfides are not transported to the upper crust, then subduction-related porphyry deposits may therefore be Cu rich and relatively Au (and potentially PGE and Te) poor (Richards, 2009).

Postsubduction porphyry deposits have been suggested to source their metals and sulfur from sulfides stored in hydrous cumulate residue from a prior subduction process, at the base of the continental crust (Richards, 2009; Hou et al., 2015). As described above these residual sulfides are likely to be enriched in Au-PGE-Te-Bi-Se due to their high D values between the sulfide and silicate melts, and the high R number of sulfides forming in a subduction zone. If these residual sulfides provide the metal source of postsubduction porphyry deposits, then these deposits may be relatively enriched in both Au (Richards, 2009) and other chalcophile and siderophile elements such as Te and PGE (Holwell et al., 2019) when compared to subduction-related porphyry Cu deposits.

However, there are reports of Au-poor postsubduction deposits, such as the Cu-Mo deposits in the Gangdese belt, Tibet (e.g., Hou et al., 2009) and the Au-poor porphyry Cu deposits in Iran (e.g., Shafiei and Shahabpour, 2008). There are also a number of subduction-related porphyry deposits that are also enriched in PGEs, Au, and Te, such as the Elatsite Cu-Au (PGE) deposit, Bulgaria, and alkalic Cu-Au (PGE) porphyry deposits in British Columbia (Thompson et al., 2001; von Quadt et al., 2005).

In this study, we use LA-ICP-MS to analyze the main sulfide minerals present in three porphyry copper deposits with different metal endowments and from contrasting tectonic settings. The Skouries Cu-Au (PGE) deposit in Greece (Hahn, 2015; Siron et al., 2016; Fig. 1C) and the Muratdere Cu-Mo (Au-Re) deposit in Turkey (Kuşcu et al., 2013; McFall et al., 2019; Fig. 1D) are postsubduction systems, whereas the El Teniente Cu-Mo deposit, Chile, is subduction related

(Camus, 2002; Fig. 1B). We compare the trace element concentrations of sulfides from these deposits with a newly compiled database of pyrite, chalcopyrite, bornite, molybdenite, sphalerite, and galena trace element data from 18 other porphyry systems from around the world (Fig. 1A; full database available as an editable file in digital App. A1). We focus on the distribution of critical and precious metals to assess which minerals preferentially host these potential by-products, and the possible control of tectonic setting on chalcophile and siderophile metal content. We also use aqua regia ICP-MS assay and Ni-S fire assay results to compare whole-rock chalcophile and siderophile element concentrations in ore samples from El Teniente, Muratdere, and Skouries and compare them with data from other porphyry systems globally to assess tectonic setting as a control on chalcophile and siderophile element abundances.

## Deposits Studied and Geologic Background

### *El Teniente Cu-Mo deposit*

The El Teniente Cu-Mo deposit is a supergiant porphyry deposit situated 70 km southeast of Santiago, Chile (Fig. 1B). It is situated on the western margin of the Andean Cordillera in the late Miocene-Pliocene central Chilean porphyry Cu belt (Fig. 1B) with an estimated premining resource of 95 million metric tons (Mt) of Cu and 2.5 Mt Mo (Camus, 2002). El Teniente has been the subject of numerous studies on its regional tectonic setting, deposit geology, and mineralization (e.g., Cannell et al., 2005; Klemm et al., 2007; Skewes and Stern, 2007; Vry et al., 2010; Spencer et al., 2015). Recent work suggests this large and complex deposit was formed between 6.3 and 4.6 Ma (Spencer et al., 2015).

El Teniente is a subduction-related deposit, and its formation has been linked to the subduction of the Juan Fernandez Ridge below the South American Plate (Skewes et al., 2002; Cooke et al., 2005; Skewes and Stern, 2007). The deposit is hosted by a series of felsic-intermediate porphyry intrusions and their host rocks, the Teniente Mafic Complex, which was emplaced between 15.2 and 7.5 Ma (Skewes et al., 2002; Skewes and Stern, 2007) and consists of mafic sills, stocks, and volcanoclastic rocks of basaltic-andesitic composition (Camus, 1975). The porphyry intrusions are enveloped and partly cut by a number of igneous and hydrothermal breccias, many of which are mineralized and which have been linked to mineralized stockwork veining in the vicinity, with similar mineralogy and alteration styles (Vry et al., 2010).

Ore grades at El Teniente are predominantly controlled by the intensity of stockwork veining (Cannell et al., 2005; Spencer et al., 2015). In this paper we use the vein chronology developed by Vry et al. (2010), with three broad paragenetic categories—premineralization veins which are associated with potassic alteration and minor sulfides; main mineralization quartz  $\pm$  anhydrite veins, which are associated with potassic to sericitic alteration, chalcopyrite, bornite, and molybdenite; and late hydrothermal stage quartz veins, which include tourmaline, sulfosalts, and minor sulfides. The first two stages were repeated several times during the evolution of the system, associated with major magmatic-hydrothermal pulses of activity (Vry et al., 2010; Spencer et al., 2015). Representative samples from main-stage vein types 6b, 7a, and 8 (Fig. 2A-C,

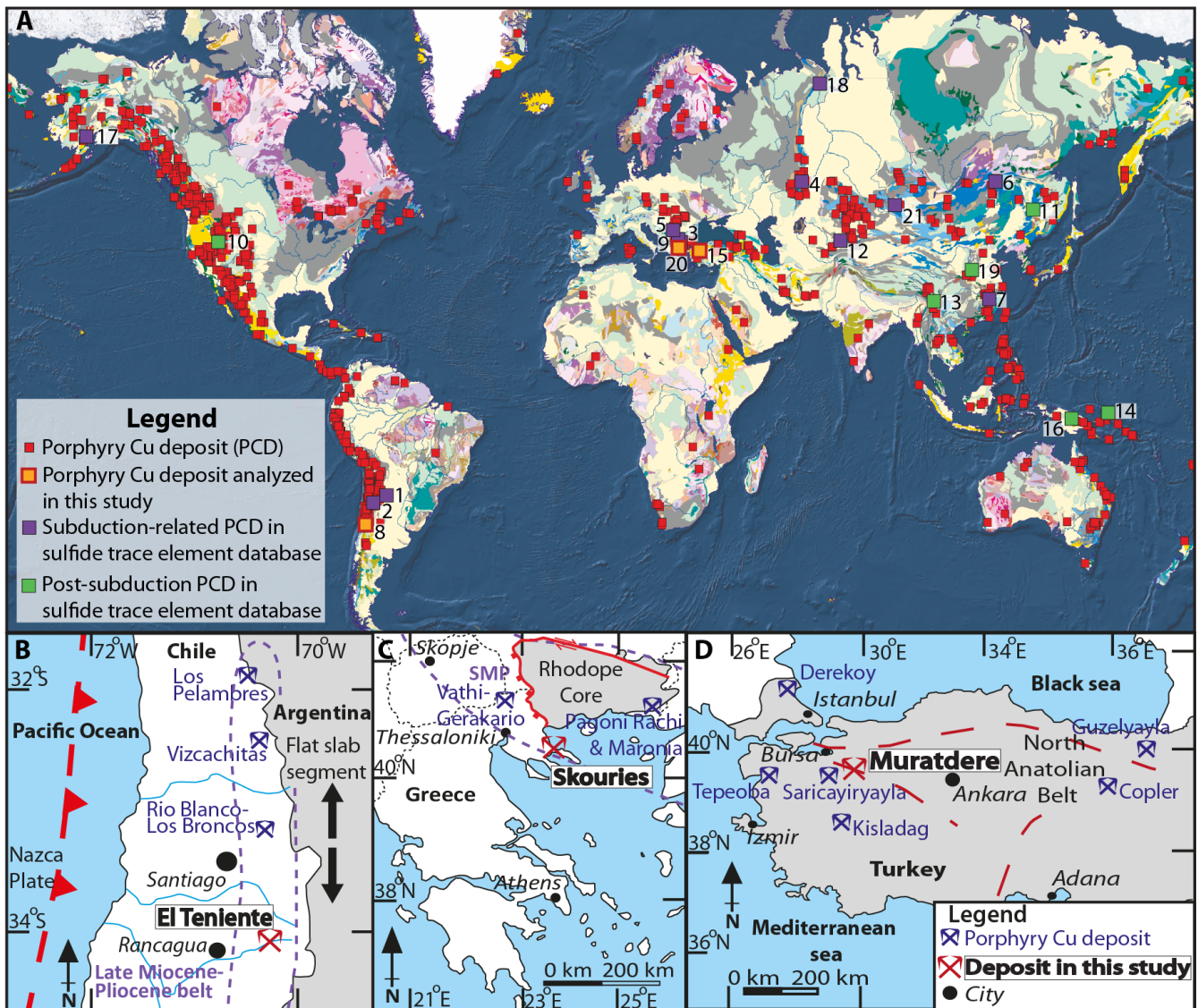


Fig. 1. A. World map showing known porphyry Cu deposits (adapted from Sinclair, 2007). Subduction-related porphyry deposits included in the global sulfide trace element database (App. A1) are highlighted in purple, postsubduction porphyry deposits in the database in green, and those sampled for this study in orange. Numbers relate to the metadata in Appendix A1. B. Location map for the El Teniente porphyry deposit (8, (A)), showing it in context of local porphyry deposits and major tectonic regions (adapted from Spencer et al., 2015). C. Location map for the Skouries porphyry deposit (20, (A)), showing it in context with the Serbomacedonian metallogenic province (SMP) and Rhodope Metamorphic Core (adapted from McFall et al., 2018). D. Location map for the Muratdere porphyry deposit (15, (A)), showing it in context with major tectonic units and local porphyry deposits (adapted from McFall et al., 2019).

respectively) were analyzed during this study as these contain all the main ore sulfide minerals, chalcopyrite, bornite, molybdenite, and pyrite (App. A2). The results provide insights into the critical metal endowment of these minerals at El Teniente, but it is important to recognize that these samples only provide a small snapshot of the system as a whole.

#### *Muratdere Cu-Au-Mo deposit*

The Muratdere Cu-Au-Mo porphyry deposit (McFall et al., 2019) is located in the Bilecik Province in western Turkey (Fig. 1D). It has a JORC-compliant Inferred Resource of 51 Mt of ore, containing 186,000 t Cu, 204,296 oz Au, 3.9 Moz Ag, 6,390 t Mo, and 17,594 kg Re (Stratex International, 2016).

The Muratdere deposit is situated within the North Anatolian belt, a Jurassic-Cretaceous ophiolitic mélangé terrane (Fig. 1D; Tekeli, 1981) within the Tethyan metallogenic belt. The Muratdere deposit has yet to be dated; however, the host intrusions are part of an E-W-trending belt of granitoids with very similar petrology, some of which have been dated as Eocene (48–54 Ma; Ataman, 1972; Delaloye and Bingol, 2000; Altunkaynak and Dilek, 2006). Eocene magmatism in this region is the result of extension following the exhumation of thickened crust (Kuscu, 2016), so Muratdere has been classified as a postsubduction porphyry system (McFall et al., 2019).

Mineralization is present in granodiorite-hosted vein stockworks. McFall et al. (2019) identified eight vein sets and

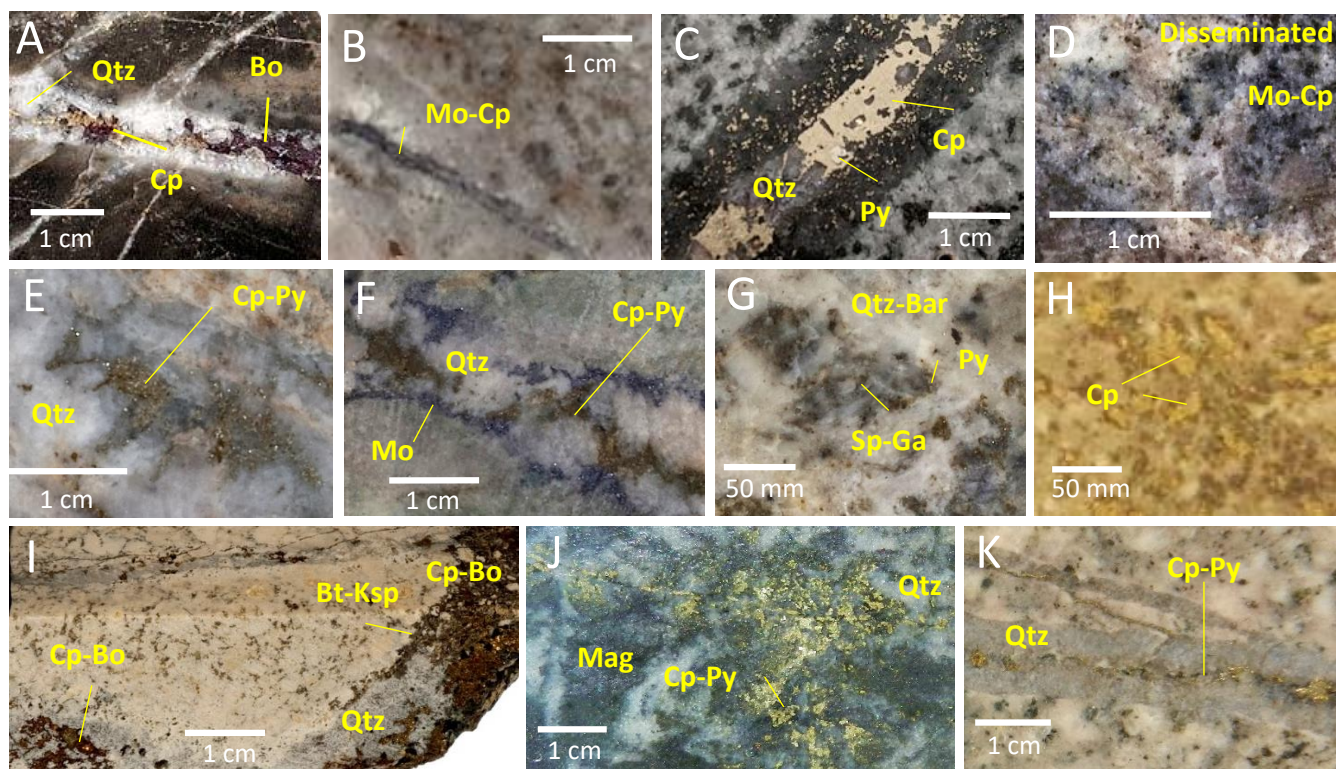


Fig. 2. Photos of vein sets analyzed from each deposit (Bar = barite, Bo = bornite, Bt = biotite, Cp = chalcopyrite, Ga = galena, Ksp = K-feldspar, Mag = magnetite, Mo = molybdenite, Py = pyrite, Qtz = quartz, Sp = sphalerite). A. El Teniente vein type 6b. B. El Teniente vein type 7a. C. El Teniente vein type 8. D. Muratdere disseminated sulfides. E. Muratdere vein set V2. F. Muratdere vein set V3. G. Muratdere vein set V5. H. Skouries disseminated chalcopyrite. I. Skouries vein set M-3. J. Skouries vein set M-4. K. Skouries vein set M-5.

this vein classification has been used in this study. The main mineralized vein sets are as follows: V2 = a quartz-chalcopyrite-pyrite vein set (Fig. 2E), V3 = a quartz-molybdenite ± chalcopyrite-pyrite vein set (Fig. 2F), and V5 = a quartz-barite-galena-sphalerite-pyrite ± chalcopyrite vein set (Fig. 2G). Significant mineralization is also hosted in disseminated sulfides (chalcopyrite-pyrite-molybdenite; Fig. 2D), which appear to represent an early stage of mineralization, dispersed in microfractures throughout the alteration halo of the deposit (McFall et al., 2019). Samples were chosen from all the mineralized vein sets, and samples with disseminated sulfides were also analyzed (App. A2). LA-ICP-MS trace element data for pyrite and molybdenite crystals from the Muratdere deposit were published in McFall et al. (2019); the new data in this study are from chalcopyrite, galena, and sphalerite.

#### Skouries Cu-Au (PGE) deposit

Skouries is a Cu-Au porphyry deposit situated in the Chalkidiki peninsula of northeastern Greece (Fig. 1C). It has a measured and indicated resource of 158 Mt at 0.49% Cu and 0.74 g/t Au for 3.8 Moz Au and 0.7 Mt Cu (Eldorado Gold Corp., 2019). The Skouries deposit is known for being PGE-enriched (Eliopoulos and Economou-Eliopoulos, 1991; Tarkian and Stribny, 1999; McFall et al., 2018) and is described in detail in Frei et al. (1995), Kroll et al. (2002), and McFall et al. (2018).

The Skouries deposit is a postsubduction system that developed in the Serbo-Macedonian metallogenic province, a subdivision of the Tethyan metallogenic belt (Fig. 1C). It is

hosted by the Vertiskos Formation, which is a part of the Serbo-Macedonian Massif. The Vertiskos Formation is separated from the Rhodope Metamorphic Core Complex by the Kerdilion detachment fault. The Rhodope Metamorphic Core Complex is a wide metamorphic dome in the northern Aegean made up of exposed middle to lower crustal rocks, which were exhumed as a result of large-scale extension (Brun and Sokoutis, 2007). Exhumation of the Rhodope Metamorphic Core Complex during the Eocene-Miocene was closely associated with postsubduction magmatism (Marchev et al., 2005; Brun and Sokoutis, 2007). The Skouries deposit has been dated at  $20.56 \pm 0.48$  Ma (zircon U-Pb; Hahn, 2015) and is part of an early Miocene alkaline magmatic episode related to extension following the exhumation of the Rhodope Metamorphic Core Complex (Fig. 1C; Siron et al., 2016, 2018).

The Skouries deposit is hosted by a series of subvertical, pipelike porphyry intrusions. These range from syenitic to monzonitic in composition, with pre-, syn-, and postmineralization intrusions present (Kroll et al., 2002; McFall et al., 2018). Mineralization is hosted in vein stockworks centered on the host intrusions. McFall et al. (2018) identified 14 vein generations, and this classification is used in this study. The veins are divided into early-stage veins, which contain minor mineralization and are crosscut by some synmineralization intrusions; main-stage veins which, are hosted by synmineralization intrusions and contain the majority of the hypogene mineralization; and late-stage veins which contain minor mineralization and postdate all synmineralization intrusions. The

majority of the hypogene mineralization is hosted in vein sets M-3, M-4, and M-5 (Fig. 2 I-K, respectively). These vein sets contain varying proportions of chalcopyrite, bornite, and pyrite, with accessory microscopic galena. These vein sets also contain a wide range of accessory minerals, including platinum group minerals (PGM), precious metal accessory minerals such as hessite and electrum, and native Au (McFall et al., 2018).

Samples were chosen from vein sets M-3, M-4, and M-5 (Fig. 2I-K). One sample, containing disseminated sulfides, was also selected (App. A2). This sample contains blebs of chalcopyrite and pyrite disseminated in the silicate groundmass at the contact between two of the premineralization porphyry units (Fig. 2H). These are interpreted to be early, premineralization sulfides, possibly associated with primary magmatism (McFall, 2016).

### Methods

Sulfide-bearing sections of the samples were prepared as polished thin sections or polished blocks for petrography and laser ablation inductively coupled plasma mass spectrometry (LA-ICP-MS). The offcuts from thin section preparation were crushed using a jaw crusher followed by an agate ring mill to produce powder for whole-rock analysis (ALS assay and Ni-S fire assay). This was done to ensure that, as far as possible, the whole-rock assay and sulfide LA-ICP-MS sampled the same sulfide assemblage.

El Teniente samples were selected from the ores collection at the Natural History Museum, London, from the Ph.D. collections of Victoria Vry and Edward Spencer. Full sample descriptions, along with more detailed petrological and geochemical analyses, are available in Vry (2010) and Spencer (2015).

#### ALS assay

Crushed samples were sent to ALS Global where aqua regia digestion was carried out on 0.5 g of each sample, followed by analysis by ICP-MS and ICP-AES (ALS method code MEMS41™). QA-QC data are summarized in Appendix A2, but accuracy was very good for all elements analyzed in certified standards (within 95% confidence range of the mean certified value) and precision is defined as good to very good (as defined by Piercey, 2014) for all elements, except Te, Se, and Bi where the percentage relative standard deviation was >10% for some duplicate analyses.

#### Ni-S fire assay

Samples were prepared for PGE and Au analyses by Ni-S fire assay and tellurium coprecipitation according to the procedures outlined in Huber et al. (2001) and McDonald and Viljoen (2006). Solutions were analyzed for PGE and Au on a Thermo X Series 2 ICP-MS system housed at Cardiff University. Accuracy, calculated from the analysis of external standards, was excellent or very good for all PGE, except Os (excellent = 0–3% relative difference (RD), very good = 3–7% RD; Piercey, 2014). Precision, calculated from duplicate analyses, was excellent for Os, very good for Pd, and good for Ir and Ru (excellent = 0–3% relative standard deviation (RSD), very good = 3–7% RSD, and good = 7–10% RSD; Piercey, 2014). Platinum, Rh, and Au have lower precision between

duplicates, probably due to nugget effects. Detection limits, blank results, and komatiite WITS1 and WMG1 standard analysis data are given in Appendix A2.

#### Sulfide LA-ICP-MS

Laser ablation analysis of sulfides was undertaken at Cardiff University, using an ESI P213 Laser Ablation System coupled to a Thermo X Series 2 ICP-MS. SEM-EDS surveys were carried out prior to LA-ICP-MS analysis to identify surface microinclusions and only sulfides without visible microinclusions were analyzed. Full methods including masses measured, interference corrections and representative time-resolved analyses (TRA) are provided in Appendix A3 and limits of detection for all elements analyzed are given in Table 1 and Appendix A1. Instrument calibration was performed using a series of five synthetic Ni-Fe-S quenched sulfide standards (composition of standards is given in Prichard et al., 2013). The standards produce five-point calibration curves for S, Ni, and Fe and three-point calibration curves for PGE, Ag, Cd, Re, Au, Cu, Co, Zn, and semimetals (further details in App. A3). Accuracy and precision for Au and PGE were checked by analyzing the CANMET Po727 Memorial standard as an unknown at the beginning and end of each sample run. Accuracy was very good to excellent for all elements (Piercey, 2014) and precision was good for all elements with an average  $2\sigma$  of 4.4 ppm. Full standard analyses are given in Appendix A1.

#### Global database

A database of published LA-ICP-MS and SIMS data from sulfides from porphyry deposits was compiled in January 2020. This consists of 1,033 sulfide analyses from 21 deposits (including those in this study, Fig. 1A), 13 of which are from subduction-related settings and eight of which are from various postsubduction settings (App. A1). These deposits have a range of metal endowments, with both Au- and Mo-rich deposits present in both tectonic categories. The minerals included in the database are bornite, chalcopyrite, galena, molybdenite, pyrite, and sphalerite. Full metadata of these analyses, including likely tectonic setting of the deposit, sulfides analyzed, limits of detection, data and tectonic categorization references are given in Appendix A1. As the trace element data are nonnormal the median is used as the center indicator and nonparametric tests are used to determine variance and correlation. Full details of statistical treatment of data and results of statistical tests are given in Appendix A4.

## Results

#### Whole-rock assay data

A summary of whole-rock results for the elements of interest is given in Table 2. Full results from ALS assay for metals and semimetals and Ni-S fire assay for PGE and Au are provided in Appendix A2 and details of statistical tests used are given in Appendix A4.

Ore samples from the Skouries deposit contain significantly more Pd, Pt, Au, Te, and Bi than those from Muratdere and El Teniente (according to Mann-Whitney-Wilcoxon and Kolmogorov-Smirnov nonparametric t-tests, confidence level 95%). Samples from Muratdere and El Teniente have statistically similar whole-rock concentrations of Pd, Pt, Te, and

Table 1. Summary of Trace Element Data for Sulfide Crystals from the Three Deposits in this Study (in ppm; full results as part of the global database in App. A1; \* interference corrected)

Deposit	Mineral	n	LOD	Au	Ag	Pd*	Pt	Te	Se	Bi
				0.01	0.17	0.07	0.02	0.17	15.00	0.05
El Teniente	Bornite	20	Median	0.01	690.44	0.42	0.02	2.32	125.60	345.59
			Max	0.03	850.52	0.70	0.03	4.73	228.56	409.32
			Min	<dl	567.37	0.23	<dl	0.76	67.44	295.46
	Chalcopyrite	55	Median	0.01	11.60	0.07	0.02	1.09	91.50	0.42
			Max	0.28	63.44	0.31	0.35	3.85	133.02	6.45
			Min	<dl	1.03	<dl	<dl	<dl	29.40	<dl
	Molybdenite	30	Median	0.15	11.16	<dl	0.02	6.86	179.17	1.03
			Max	2.12	119.96	<dl	0.18	81.42	636.14	477.63
			Min	<dl	2.10	<dl	<dl	3.91	61.19	<dl
	Pyrite	31	Median	0.01	0.17	0.07	0.02	0.41	43.16	0.24
			Max	0.07	167.20	0.17	0.08	5.67	113.39	3.17
			Min	<dl	<dl	0.07	<dl	<dl	21.84	<dl
Muratdere	Chalcopyrite	11	Median	0.03	7.78	0.02	0.02	0.58	95.35	0.88
			Max	0.47	98.13	<dl	0.04	2.63	131.04	11.15
			Min	<dl	1.43	<dl	<dl	<dl	58.21	0.15
	Galena	8	Median	0.07	165.87	<dl	<dl	0.88	303.91	3.07
			Max	0.12	417.52	<dl	<dl	2.76	551.97	5.82
			Min	0.04	94.83	<dl	<dl	<dl	158.24	1.46
	Sphalerite	3	Median	<dl	0.71	<dl	<dl	<dl	<dl	<dl
			Max	<dl	1.12	<dl	<dl	<dl	<dl	<dl
			Min	<dl	0.32	<dl	<dl	<dl	<dl	<dl
Skouries	Bornite	21	Median	0.01	289.12	0.07	0.02	20.08	608.42	3,358.92
			Max	5.93	583.98	0.39	0.09	96.55	772.04	3,855.83
			Min	<dl	1.43	<dl	<dl	0.17	245.00	0.23
	Chalcopyrite	124	Median	0.01	2.86	0.07	0.02	1.62	261.98	2.53
			Max	0.23	228.65	3.99	0.15	14.76	993.95	26.48
			Min	<dl	<dl	<dl	<dl	<dl	62.75	0.09
	Pyrite	68	Median	0.01	0.17	0.07	0.02	3.03	40.91	0.26
			Max	1.17	16.69	4.25	0.04	47.99	361.39	38.41
			Min	<dl	<dl	<dl	<dl	<dl	<dl	<dl

Bi, but Muratdere contains significantly more Au (Fig. 3). All three deposits have statistically similar concentrations of Ag and Se, despite the Skouries deposit samples having a larger spread of Se concentrations. The disseminated sulfide sample from Skouries (SK4) contains less Rh, Pt, Pd, Au, Cu and more Te than the vein samples; however, there are no other statistically significant differences in precious or critical metal concentrations in ore samples between paragenetic stages within any of the deposits.

Whole-rock ore samples from all three deposits show a statistically significant (Spearman coefficient >0.70) positive correlation between Bi and Te (statistical test details in App. A4; Fig. 4B). The El Teniente ore samples display a strong positive correlation (Spearman co-efficient >0.70) between Se-Te, Se-Bi and Ni-Co; a strong negative correlation (Spearman coefficient <-0.70) between Au-Se and Au-Bi; and a moderate positive correlation (Spearman coefficient >0.60) between Ag-Se, Ag-Te, and Te-Bi (App. A4). Ore samples from the Muratdere deposit have a strong positive correlation between Au-Ag, Ni-Se, and Te-Bi (Fig. 4A-B, App. A4). The Skouries deposit has a moderate positive correlation between Ag-Se and a strong positive correlation between Te-Bi, Pt-Pd, Ag-Bi, and Se-Te (Fig. 4B-C, App. A4).

When all the whole-rock PGE data are considered together Au and the PPGE (total concentration of Pd, Pt, and Rh) have a moderate positive correlation (Spearman coefficient 0.61), and Pd and Pt have a strong positive correlation (Spearman coefficient 0.87). Interestingly, IPGE (total concentration Ir,

Ru, and Os) do not correlate with PPGE (Spearman coefficient 0.43). When the data for each deposit are analyzed individually El Teniente shows very strong positive correlation (Spearman coefficient >0.85) between Pt-Se, Pt-Te, Pt-Bi and Pd-IPGE, strong positive correlation between IPGE-PPGE and strong negative correlation between Pt-Au. Palladium and Pt do not correlate in El Teniente (Spearman coefficient 0.14; Fig. 4C). Muratdere, in contrast, shows very strong positive correlation between Pd-Pt (Fig. 4C) and very strong negative correlation between Co-Pt and Co-Pd. Skouries shows a very strong positive correlation between Pd-Pt and a strong negative correlation between IPGE-Te and PPGE-Se. IPGE and PPGE do not correlate in Skouries.

Skouries samples are enriched in PPGE, in particular Pd, relative to IPGE with median total PPGE/IPGE of 118.7 and Pd/Pt of 20.3. Skouries also has a median (Pd + Pt)/Au of 0.17. Muratdere, in contrast, has a median (Pd + Pt)/Au of 0.02, with median total PPGE/IPGE of 10.7 and Pd/Pt of 0.4, showing it is more depleted in PPGE and Pd compared to IPGE than Skouries, with a higher relative Au content. El Teniente has more equal concentrations of PPGE and IPGE, with a median Pd/Pt of 1.1 and median total PPGE/IPGE of 5.2. El Teniente is also relatively depleted in Au, with a median (Pd + Pt)/Au of 0.28.

#### LA-ICP-MS of sulfides

A summary of the precious and semimetal contents of the sulfides analyzed during this study is found in Table 1, with full

Table 2. Summary of Whole-Rock Assay Data for the Chalcophile and Siderophile Elements of Interest from the Three Deposits in this Study (full results in App. A2; ° data from Ni-S fire assay)

Deposit	<i>n</i>		Ag ppm	Se ppm	Te ppm	Bi ppm	Cu ppm	Mo ppm	Fe %	S %	Re ppm	Co ppm
El Teniente	6 (6)	Median	2.51	5.65	0.115	0.315	14,050	128.75	2.895	2.715	0.046	11.05
		Max	15.45	12.7	0.3	12.95	45,800	2,640	6.86	7.86	0.954	49.5
		Min	1.55	2.1	0.06	0.1	12,050	4.46	2.39	2.25	0.001	2.4
Muratdere	10 (20)	Median	1.56	3.5	0.12	0.12	5,180	93.8	2.38	5.06	0.148	11.5
		Max	42.5	17.8	3.33	1	14,650	1,720	7.68	8.54	1.945	75.7
		Min	0.08	0.6	0.02	0.01	84.9	1.17	0.68	2.78	0.002	7.9
Skouries	13 (12)	Median	1.5	10.1	1.38	2.25	13,700	2.7	9	2.38	0.007	10.1
		Max	48.4	74.3	6.48	222	112,000	442	14	5.12	1.615	70.4
		Min	0.27	1.3	0.21	1.08	36.1	0.59	1.79	0.44	0.001	2.1
Deposit	<i>n</i>		Ni ppm	Pb ppm	Zn ppm	Os ppb	Ir ppb	Ru ppb	Rh ppb	Pt ppb	Pd ppb	Au ppb
El Teniente	6 (6)	Median	12	2.15	29.5	0.01	0.02	0.92	0.16	1.44	2.23	11.70
		Max	28.9	9.3	37	0.05	0.02	1.55	0.44	5.00	10.72	20.79
		Min	5.2	1.9	13	0.01	0.01	0.51	0.10	0.41	1.93	5.73
Muratdere	10 (20)	Median	2.8	10.9	88	0.03	0.03	0.11	0.13	1.24	0.54	126.84
		Max	8.7	15,100	51,400	0.06	0.08	0.59	0.33	4.84	2.72	803.82
		Min	1.1	4	15	0.01	0.02	0.09	0.08	0.75	0.10	2.74
Skouries	13 (12)	Median	18.2	46.7	40	0.02	0.02	0.46	0.22	3.81	93.60	462.75
		Max	28.6	142	144	0.06	0.04	2.22	0.56	17.25	1,012.63	1,734.13
		Min	8.6	11.9	2	0.00	0.01	0.13	0.03	0.34	0.22	17.12

results available as part of the global database in Appendix A1. Comparisons are drawn with the global sulfide database for each sulfide type. However, apart from this study, bornite analyses are only available from the Elatsite subduction-related Cu-Au porphyry deposit (Cook et al., 2011) so comparisons in this case can only be made between Elatsite, Skouries, and El Teniente (no bornite was observed at Muratdere). Statistically significant enrichments and correlations are outlined

below, and full statistical analysis of the data is available in Appendix A4.

*El Teniente:* Sulfides from El Teniente were analyzed from six samples, representing a range of vein types and paragenetic stages. A total of 20 bornite crystals, 55 chalcopyrite crystals, 30 molybdenite crystals, and 31 pyrite crystals were analyzed, although not all sulfide types were present in all samples (App. A2).

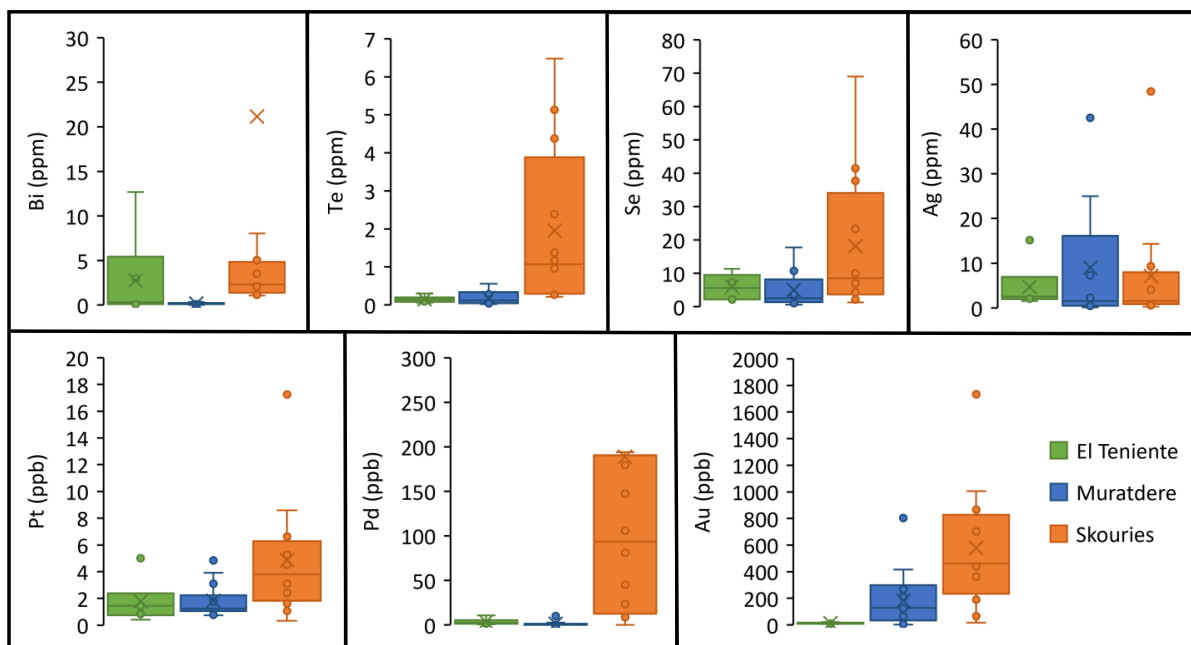


Fig. 3. Box plots showing the concentration of critical and precious metals in whole-rock ore samples from the El Teniente (green), Muratdere (blue), and Skouries (orange) deposits. The box represents the range between the 1st and 3rd quartile, with the central line indicating the median and the cross representing the arithmetic mean. The whisker lines represent the range between the 10th and 90th percentile and circles represent outliers beyond those.

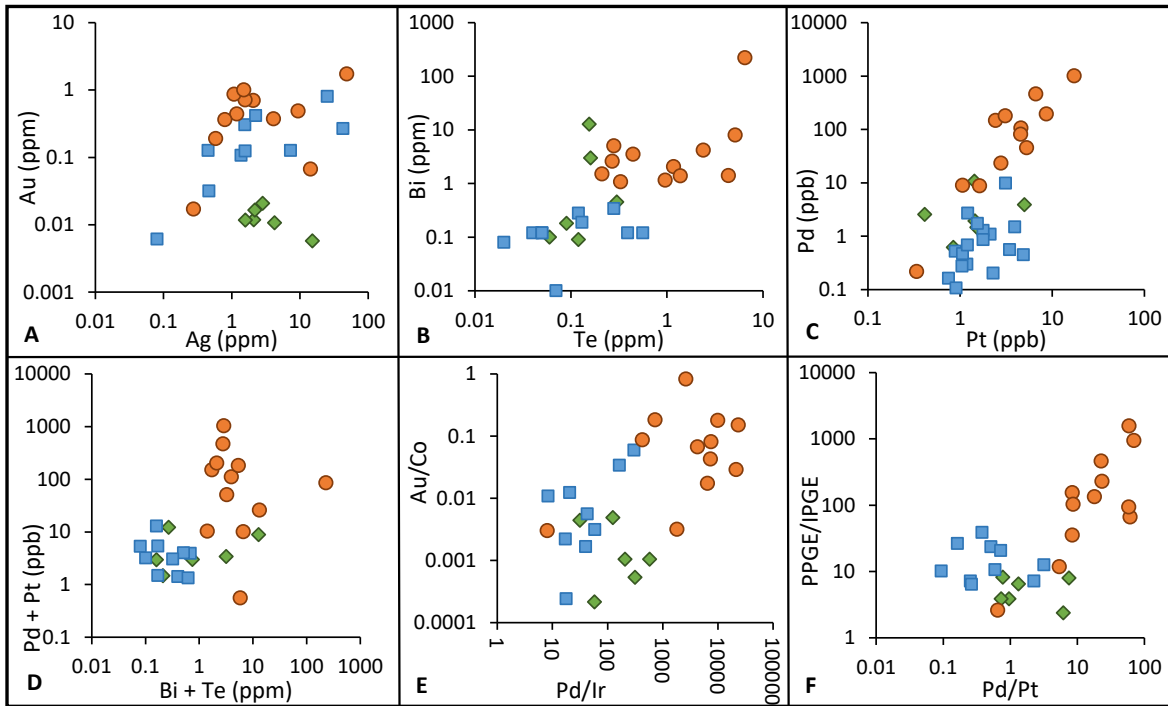


Fig. 4. Biplots illustrating the relationship between key precious and semimetals in whole-rock samples in the El Teniente (green triangles), Muratdere (blue squares), and Skouries deposits (orange circles).

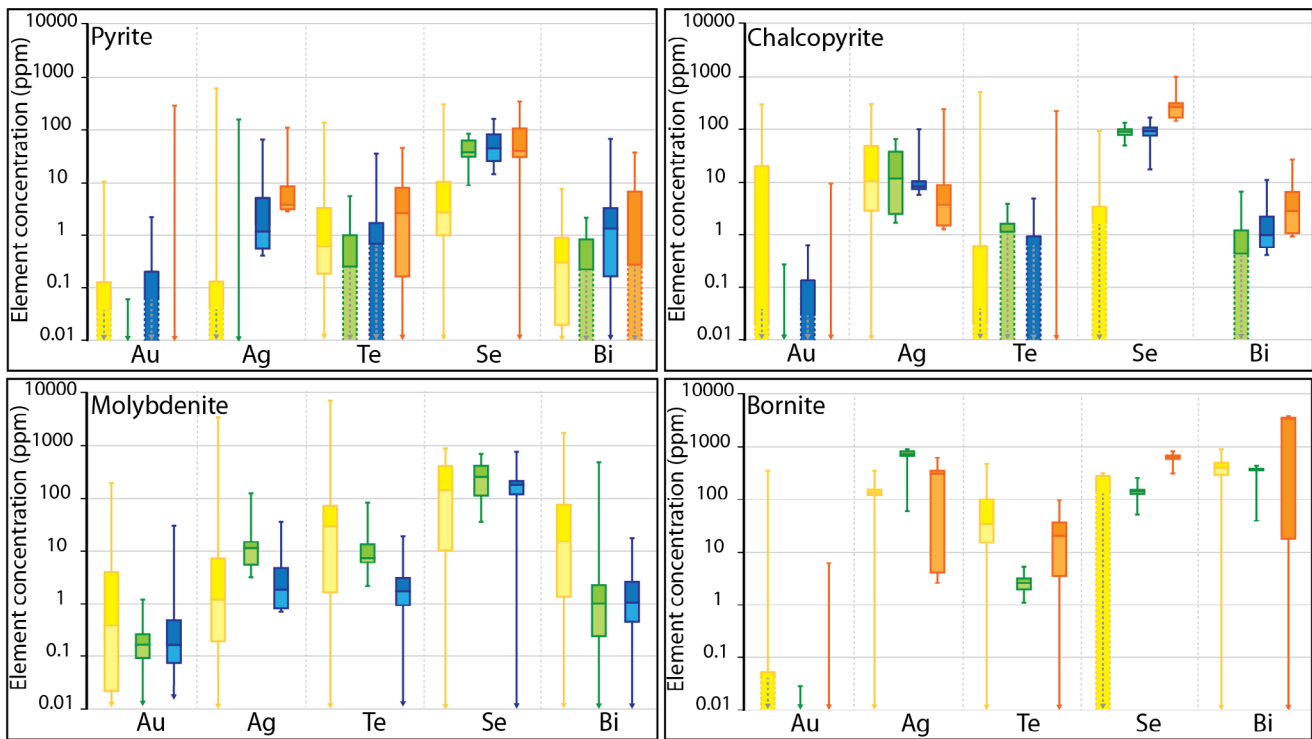


Fig. 5. Logarithmic box plots illustrating the precious and critical metal concentrations of the main sulfide ore minerals from El Teniente (green), Muratdere (blue), and Skouries (orange) deposits, compared to those in the same sulfides in global porphyry Cu deposits (yellow, data from global database, App. A1). The box represents the range between the 1st and 3rd quartile, with the central line indicating the median and whiskers represent range between minimum and maximum values. A downward arrow in place of a minimum indicates the minimum was below detection limit, and the dotted lines and arrows on the box indicate the median or 1st quartile was also below detection limit. Note that bornite global data are from Elatsite only.



The bornite from El Teniente generally contains significantly more Ag and less Te than that from Skouries and Elatsite, and lower Se concentrations than Skouries (Fig. 5). All the bornite crystals analyzed from El Teniente have Pd concentrations above the detection limit (0.07 ppm), with a median of 0.42 ppm and a maximum of 0.7 ppm. Platinum was detected (>0.02 ppm) in three analyses, with a maximum of 0.03 ppm. Chalcopyrite from El Teniente contains significantly less Bi than observed at Muratdere and Skouries (Fig. 7, App. A4). Palladium was detected in four analyses, with a maximum of 0.31 ppm, and Pt was detected in 11 analyses of chalcopyrite, with a maximum of 0.35 ppm. Molybdenite trace element concentrations from El Teniente are not statistically significantly different from those in other porphyry deposits. Seven molybdenite analyses recorded Pt concentrations above detection, with a maximum concentration of 0.18 ppm. Pyrite from El Teniente contains significantly more Se than porphyry deposits globally. Three pyrite analyses returned Pd concentrations above detection, with a maximum of 0.31 ppm. Pt was detected in just two pyrite analyses, with a maximum of 0.08 ppm.

**Muratdere:** Sulfides from Muratdere were analyzed from six samples of the three main mineralized vein sets. Chalcopyrite ( $n = 11$ ), galena ( $n = 8$ ), and sphalerite ( $n = 3$ ) were analyzed as part of this study; data from pyrite ( $n = 47$ ) and molybdenite ( $n = 71$ ) were reported by McFall et al. (2019).

Chalcopyrite crystals from Muratdere contain significantly more Se than from other porphyry deposits (Fig. 5). One chalcopyrite crystal exhibited a Pt concentration above detection (0.04 ppm). Muratdere galena crystals all contain detectable Au, but no Pd. Sphalerite crystals in Muratdere are very trace element poor with all precious and semimetal concentrations below detection limit. Pyrite crystals in Muratdere contain significantly more Se and Bi than those in global porphyry deposits, with significant differences between paragenetic stages within the deposit (McFall et al., 2019). One pyrite crystal returned Pd concentration above detection (0.27 ppm) and one returned Pt above detection (0.04 ppm). Three molybdenite crystals returned Pd values above detection (0.54, 0.74, and 0.78 ppm) and 22 returned Pt values above detection limit, with a maximum of 2.25 ppm and a median of 0.05 ppm Pt.

**Skouries:** Chalcopyrite ( $n = 124$ ), pyrite ( $n = 68$ ), and bornite ( $n = 15$ ) were analyzed in 12 samples representing the main mineralization-carrying veins in the Skouries deposit, and in one sample of disseminated sulfides along the contact between two host porphyry dike units (App. A2).

Bornite from Skouries contains significantly more Bi than that from El Teniente or Elatsite (Fig. 5). It also contains significantly less Ag than bornite from El Teniente. Palladium was detected in four analyses, with a maximum concentration of 0.39 ppm; Pt was detected in one crystal with a concentration of 0.09 ppm. Chalcopyrite from Skouries contains significantly more Se than is typical for porphyry systems globally (Fig. 5). Twelve analyses yielded Pd concentrations above the detection limit, with a maximum concentration of 4.25 ppm. Platinum was detected in 10 analyses, with a maximum of 0.15 ppm. Pyrite from Skouries contains statistically significantly more Ag, Te, and Se than is typical of porphyry systems globally (Fig. 5, App. A4). Palladium was detected in 12 pyrite

analyses with a maximum of 4.25 ppm and Pt was detected in two crystals, with a maximum of 0.04 ppm.

## Discussion

### *Sulfides as precious and critical metal hosts in porphyry deposits*

A combination of data from this study and the global database allows an assessment of the potential of different sulfide types as reservoirs for critical and precious metals in porphyry-type ore deposits. This can inform geometallurgy and also gangue disposal as some of these elements, such as Se, can be harmful to the environment in high concentrations.

The main Cu ore minerals in porphyry deposits are chalcopyrite and bornite. Bornite contains significantly more bismuth than other sulfide types, with Bi concentrations in the global database between 0.23 and 3,385 ppm, with a median of 383 ppm (Fig. 6E, App. A1). The time-resolved analytical traces of Bi in bornite are smooth and match those of S and Cu (App. A3), suggesting that Bi is hosted in solid solution. Bornite can also contain 10s of ppm Te and 100s of ppm Se, with bornite crystals in the global database containing between 0.17 and 96.5 ppm and 67 to 772 ppm, respectively (Fig. 6C-D). Bornite also contains significantly more Ag than other sulfide types (Fig. 6B).

Chalcopyrite is generally trace element poor due to its covalent bonding and complex structure (George et al., 2018). Thus, its trace element composition is very dependent on co-crystallizing phases, with trace element enrichment only seen in the absence of other sulfides. This behavior is observed in this study, where chalcopyrite in an assemblage with bornite contains lower trace element concentrations than that which has no accompanying sulfides. Chalcopyrite can, however, contain 10s ppm Te, with up to 143 ppm Te recorded in the global database (Fig. 6D) and can contain both Se and Ag at elevated levels, up to 994 and 218 ppm, respectively (Fig. 6C-B).

Chalcopyrite and bornite do not contain significant concentrations of Au, with 70% of chalcopyrite and bornite analyses below detection limit, 28% below 1 ppm Au, and with a maximum Au concentration of 9.7 ppm (Fig. 6A). Experimental work has shown that Au solubility in bornite drops from 100s ppm at 600°C to 10s of ppm at 400°C (Simon et al., 2000). It has been suggested that the Au content of porphyry Cu deposits is at least partially controlled by the Au saturation of chalcopyrite and bornite at high temperature during hypogene ore formation, and then as these sulfides cool the excess Au forms native Au at sulfide boundaries (Kesler et al., 2002).

Molybdenite is the other main ore mineral present in porphyry copper deposits. Molybdenite crystals can be trace element rich and commonly contain mineral inclusions and microinclusions (e.g., Ciobanu et al., 2013; Pasava et al., 2016). Tellurium and Bi are commonly hosted in molybdenite crystals as inclusions of Te-Bi minerals and therefore have very variable concentrations, with maximums of 1,718 ppm Bi and 6,219 ppm Te in molybdenite crystals from the global database (Fig. 6D-E). These mineral inclusions are observed in the Kalmakyr porphyry Cu deposit, Uzbekistan, and Hilltop porphyry-epithermal system, United States (Ciobanu et al., 2013; Pasava et al., 2016), and are interpreted to be present in

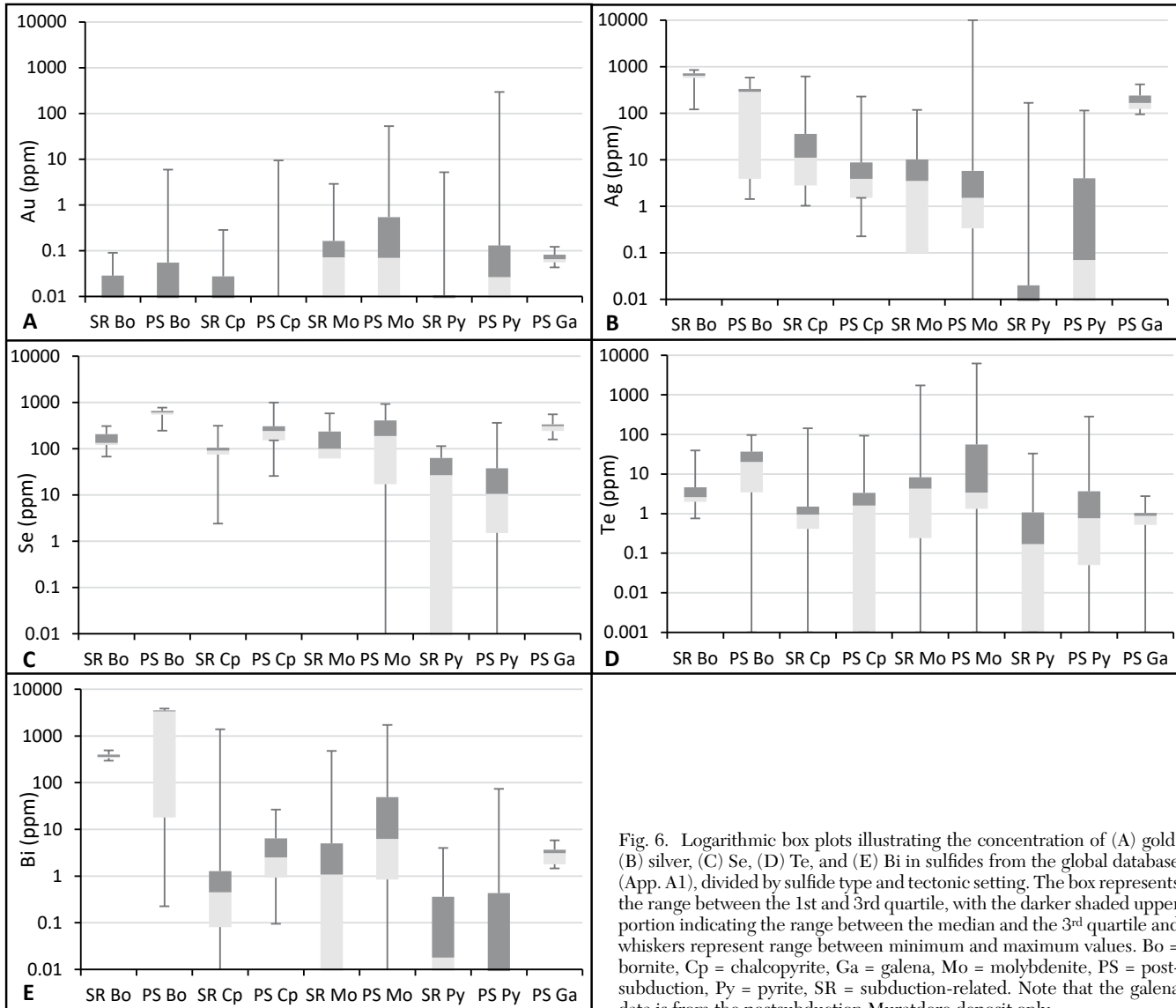


Fig. 6. Logarithmic box plots illustrating the concentration of (A) gold, (B) silver, (C) Se, (D) Te, and (E) Bi in sulfides from the global database (App. A1), divided by sulfide type and tectonic setting. The box represents the range between the 1st and 3rd quartile, with the darker shaded upper portion indicating the range between the median and the 3rd quartile and whiskers represent range between minimum and maximum values. Bo = bornite, Cp = chalcopyrite, Ga = galena, Mo = molybdenite, PS = post-subduction, Py = pyrite, SR = subduction-related. Note that the galena data is from the postsubduction Muratdere deposit only.

the Muratdere deposit, Turkey (McFall et al., 2019) and in the El Teniente deposit due to the irregular time-resolved signals for these elements during LA-ICP-MS (App. A3). Selenium concentrations in molybdenite are variable, varying from below detection limit to 100s ppm (Fig. 6C). Unlike Te and Bi, Se has smooth LA-ICP-MS signals (App. A3), suggesting that it is present in solid solution or as homogeneously distributed nanoinclusions. Selenium concentrations have been found to be highly variable across individual molybdenite crystals, and this has been interpreted to reflect different stages of hydrothermal growth (Ciobanu et al., 2013; Pasava et al., 2016; McFall et al., 2019). Molybdenite crystals can contain high concentrations of Au, with a maximum value in the database of 53 ppm (Fig. 6A). However, 14% of molybdenite analyses are still below detection limit and 44% of analyses are below 1 ppm Au. Anomalously high Au concentrations in molybdenite are likely the result of accidental analysis of Au-bearing mineral microinclusions, which are common in molybdenite crystals (e.g., Pasava et al., 2016).

Pyrite also makes up a large proportion of the sulfides present in many porphyry systems and can host significant trace element concentrations, including critical metals (Keith et al., 2017a). Pyrite in the global database contains between 0.01 and 123 ppm Te (Fig. 6D). Tellurium has been suggested to be preferentially incorporated into As-rich pyrite, in a similar fashion to Au (Keith et al., 2018); the incorporation of As into the pyrite crystal lattice creates crystal defects, which allows the incorporation of trace elements as nanoinclusions, and the substitution of larger radii ions, such as Au or Te, for Fe (Abraitis et al., 2004; Chouinard et al., 2005; Reich et al., 2005; Deditius et al., 2014). However, there is no correlation between Te and As in the porphyry pyrite in this database and the LA-ICP-MS signals for Te in this study (App. A3) show an irregular pattern, consistent with the presence of microinclusions of Te phases. Thus, we conclude that porphyry system pyrite with Te concentrations of >10 ppm is likely to contain native Te or telluride mineral microinclusions. Pyrite in porphyry deposits also contains up to 100s ppm Se, with a

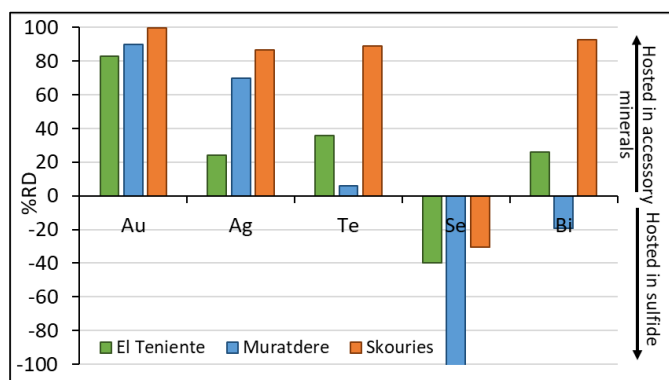


Fig. 7. Graph showing the average percentage relative difference (%RD) between calculated and measured whole-rock concentrations of critical and precious metals in each deposit. Concentrations of the element in sulfides were used in conjunction with sample mineralogy to calculate the whole-rock concentration of the element if it was entirely hosted in sulfide. The relative difference was then calculated using the equation  $((X_{\text{meas}} - X_{\text{calc}})/X_{\text{meas}}) \times 100$ , where  $X_{\text{meas}}$  is the measured whole-rock concentration and  $X_{\text{calc}}$  is the calculated whole-rock concentration. 100% means all the element is hosted in accessory minerals and 0% means it is hosted entirely in sulfides. Negative %RD reflects an error in sulfide abundance calculation but shows that all the element is hosted in the sulfide.

range in the database from below detection limit to 361 ppm (Fig. 6C).

Galena is found as a minor phase in porphyry ore. Where present, it can contain very high levels of Se, with up to 347 ppm from Muratdere (this study, Fig. 6C) and 4 wt % from EPMA analysis of samples from Skouries (McFall et al., 2018). This is due to clausthalite [PbSe] forming a solid solution with galena [PbS] above 300°C (Liu and Chang, 1994; George et al., 2015), with clausthalite reported as an accessory mineral in some deposits (George et al., 2015; McFall et al., 2018). Galena can also host significant amounts of silver, with between 94 and 403 ppm measured in galena crystals from the Muratdere deposit (Fig. 6B). Because of this, other sulfides coprecipitated with galena are Se and Ag depleted (George et al., 2016); however, galena is minor in hypogene porphyry mineralization so it is unlikely to be a significant reservoir of these metals in such domains.

#### Accessory minerals as critical and precious metal hosts

Gold is below detection limit in the majority of analyses reported in the global database, even those from Cu-Au porphyry deposits (Fig. 6A). Platinum group elements are also commonly below detection limits, with those sulfides which do contain Pd or Pt above detection limits rarely exceeding 1 ppm. This includes sulfides from the Kalmakyr and Skouries deposits, which are known to be PGE enriched and have >1 ppm Pd and Pt in whole-rock samples (Economou-Eliopoulos and Eliopoulos, 2000; Pašava et al., 2010). When detected in LA-ICP-MS analyses, Au, Pd, and Pt do not exhibit smooth laser ablation signals (App. A3), suggesting that they are present within microscopic platinum group mineral (PGM), native Au or electrum inclusions. This is supported by the association of high Pd concentrations with high Bi and Te, which also commonly occur in these phases. Precious metal accessory minerals are common in porphyry deposits, with electrum

almost ubiquitous in Cu-Au systems (Kesler et al., 2002). Other accessory minerals reported include Ag, Te, Bi, and Se minerals, such as hessite [Ag<sub>2</sub>Te], wittichenite [Cu<sub>3</sub>BiS<sub>3</sub>], and clausthalite [PbSe]. PGE-enriched porphyry deposits all contain accessory PGM such as merenskyite [(Pd,Pt)(Te,Bi)<sub>2</sub>] and sopcheite [Ag<sub>4</sub>Pd<sub>3</sub>Te<sub>4</sub>] (e.g., Tarkian et al., 2003; Augé et al., 2005; Bogdanov et al., 2005; Pašava et al., 2010; McFall et al., 2018) and so it is likely that these are the main hosts of PGE in porphyry systems.

Mass balance calculations were performed for the samples analyzed in this study to test whether the majority of the elements of interest (Au, PGE, Ag, Te, Se, and Bi) are more likely to be present in the major sulfides, or in nonsulfide accessory minerals. This was done by estimating potential metal concentrations in whole-rock samples by using the equation below:

$$X_{\text{AuWR}} = \rho_{\text{sul}}/\rho_{\text{wr}} \cdot Y \cdot X_{\text{AuSul}}$$

where  $X_{\text{AuWR}}$  is the concentration of Au, or the element of interest, in the whole rock;  $\rho_{\text{sul}}$  is the density of the sulfide;  $\rho_{\text{wr}}$  is the density of the whole rock;  $Y$  is the estimated volume percentage of sulfide in the sample as a fraction and  $X_{\text{AuSul}}$  is the concentration of Au in the sulfide as a weight fraction.

This estimate was then compared against the measured whole-rock concentrations (Fig. 7; full method and results in App. A5). These calculations show that Au is almost all hosted in accessory minerals in all the deposits in this study, with 10% of Au hosted in sulfides in Muratdere and 17% in El Teniente. Muratdere and Skouries host the majority of Ag (~70–87%) in accessory minerals while El Teniente hosts ~80% of Ag in major sulfides. Accessory hessite [Ag<sub>2</sub>Te] and electrum [Au<sub>x</sub>Ag<sub>1-x</sub>], along with rare native Au, are the most likely accessory mineral hosts for Au and Ag; these have been documented in Skouries (McFall et al., 2018) and are probably present in Muratdere as well.

The mass balance analysis suggests that most of the Te and Bi at Skouries is hosted in accessory minerals (Fig. 7); this is supported by the presence of Bi-Te accessory minerals in almost all mineralized samples (McFall et al., 2018). Conversely, for Muratdere and El Teniente, Te and Bi are at least partly hosted in the major sulfides. Most of the calculated whole-rock Se concentrations are greater than the measured concentrations in all three porphyry systems, indicating that almost all the Se is hosted by the major sulfides.

However, as discussed above, elements hosted within major sulfides may still be hosted as microinclusions of accessory minerals or the native element, rather than in solid solution. These conclusions are supported by element correlations in the whole-rock data and the time-resolved analyses (TRA) of LA-ICP-MS analyses (App. A3). The TRA for Te, Au, and PGE, where present, are irregular with distinct peaks, potentially representing microphases rich in these elements. Bismuth has irregular TRA traces in all sulfides, except bornite, where it mirrors S. Silver also varies between irregular and smooth TRA traces between sulfides and it is likely these elements can be present both as microinclusions and in solid solution. Selenium almost always follows a smooth TRA pattern, mirroring S, showing it to be in solid solution (App. A3). The positive correlation between Bi-Te in whole-rock samples may be because the Bi and Te in whole rock are in Bi-Te-bearing minerals and/or as microinclusions of such minerals

in sulfides (Fig. 4B; App. A3). Au and Ag are positively correlated in the Muratdere deposit and show a broad positive relationship in the Skouries deposit (Fig. 4A), which may be due to the presence of electrum as the main Au host mineral. However, the Skouries deposit also contains Ag-only accessory minerals hessite, empressite, stützite, and volynskite as well as Au-Ag minerals electrum and sylvanite and native Au (McFall et al., 2018), which will affect the correlation of Au and Ag. Gold and Ag have very similar solubility and depositional controls in porphyry deposits (Kesler et al., 2002) so it is likely this correlation is more due to spatial coincidence, especially as the Au/Ag in Skouries whole rock (0.3) is not consistent with that recorded for electrum in this deposit (Au/Ag = 17; McFall et al., 2018).

Palladium and Pt show a strong positive correlation in Skouries (Fig. 4C; App. A4), which is consistent with their occurrence in PGM, particularly merenskyite [(Pd,Pt)(Te,Bi)<sub>2</sub>], although many of the PGM present are Pd-only species (McFall et al., 2018). Muratdere also shows a strong positive correlation between Pd and Pt (Fig. 4C; App. A4), although no PGM have been observed at Muratdere to date (McFall et al., 2019). Although there is a moderate positive correlation between Au and PPGE when considering all deposits together, in each individual deposit there is no relationship between Au and Pd or Pt, suggesting that they are controlled by different processes. Similarly, mineralogical observations in Skouries have shown Au-bearing minerals are not always coeval with PGM (McFall et al., 2018).

The presence of PGM, more commonly associated with magmatic sulfide deposits, in porphyry systems is something of a paradox. It has been suggested that "excess" Au, Te, Bi, and PGE form accessory minerals once sulfides are fully saturated, or during cooling as precious metal accommodation (as a solid solution) in Cu sulfides drops with falling temperature (Kesler et al., 2002). However, many of the chalcopyrite and bornite crystals in PGE- and Au-rich porphyry deposits contain no detectable Au or PGE, despite the presence of native Au and PGM (McFall et al., 2018). Similarly, bornite from Skouries, although containing elevated Bi, is not at saturation with respect to Bi (Sugaki et al., 1981) despite the presence of Bi minerals in the same veins.

It has been proposed that PGM in porphyry deposits may form by a Bi-Te collector process, in which an immiscible semi-metal melt scavenges Pd, Pt, and some Au from the surrounding hydrothermal fluid before cooling to form PGM (McFall et al., 2018; Holwell et al., 2019; Helmy and Botcharnikov, 2020). Bi-Te melts can exist down to temperatures of 266°C (Ciobanu et al., 2005) and experimental work has shown that a Bi melt can exsolve from a highly saline fluid (Tooth et al., 2008, 2011; Cockerton and Tomkins, 2012). This is supported by the morphology of PGM in porphyry deposits, which are present as ovoid, compound droplet inclusions within hydrothermal quartz crystals (Ciobanu et al., 2005; McFall et al., 2018), and the presence of extremely saline brines has been documented at Skouries (McFall, 2016).

Interestingly, given that the majority of PGM are Te and Bi minerals, there is no clear relationship between Pd + Pt and Te or Bi in any of the deposits studied (Fig. 4D). Skouries contains higher concentrations of both PGE and semimetals than the other deposits, but they do not correlate. This may be

because Te is also present in other minerals that do not contain PGE, such as hessite, and Bi is concentrated in bornite as well as in PGM. This means that the whole-rock Bi or Te concentration of a sample cannot be used as a proxy for PGE grade, although PGE-enriched porphyry deposits are still more Bi-Te rich on a per-deposit scale. Similarly, there is no systematic relationship between Au and Pd + Pt in porphyry ore samples meaning that Au grade cannot be used as a PGE grade proxy either.

#### *What control does tectonic setting have on the precious and critical metal content of porphyry Cu deposits?*<sup>2</sup>

The global porphyry sulfide database has been divided into analyses from subduction-related deposits and postsubduction deposits to see if there are any significant trace element differences in sulfides between the two tectonic environments (Fig. 6, references for tectonic categorization of individual porphyry systems in App. A1). However, it should be noted that the effects of fluid conditions (e.g., temperature, oxidation state, pH) have not been taken into account and that care should be taken interpreting these results as many chalcophile and siderophile elements (namely Te, Au, PGE, and some Bi) are predominantly present in nonsulfide accessory minerals.

All sulfide types in subduction-related settings are statistically significantly enriched in Co. Silver is significantly enriched in subduction-related porphyry chalcopyrite, bornite, and molybdenite (Fig. 6B), Se is significantly enriched in subduction-related pyrite (Fig. 6C) and Cu is significantly enriched in subduction-related pyrite and molybdenite.

Bismuth is statistically significantly enriched in every type of sulfide in postsubduction porphyry deposits, as are Sb and Te (Fig. 6D-E). Selenium is significantly enriched in chalcopyrite, molybdenite, and bornite in postsubduction porphyries (Fig. 6C), and Ag is significantly enriched in pyrite (Fig. 6B). However, as shown through the mass balance calculations above, many of the elements of interest are not hosted in sulfides and so whole-rock data are needed to fully understand the differences between tectonic environment.

The two postsubduction deposits (Muratdere and Skouries) have higher whole-rock Au concentrations than El Teniente, but there is no significant difference in the other chalcophile and siderophile elements from whole-rock analysis (Fig. 3). There is, however, a striking difference between the Skouries deposit and the other two deposits, with Skouries samples containing significantly higher concentrations of Pt, Pd, Te, and Bi than both Muratdere and El Teniente (Fig. 3). The whole-rock PGE and Au analysis from the deposits in this study were compared to other porphyry ore samples, which have been analyzed for the full suite of PGE and Au (Fig. 8). These include porphyry systems known to be PGE enriched—the Elatsite porphyry Cu-Au deposit, Bulgaria (subduction-related; Augé et al., 2005); the Galore Creek, Lorraine, Mt. Milligan and Mt. Polley porphyry Cu-Au deposits, British Columbia (subduction-related; Thompson et al., 2001); the Kalmkyr porphyry Cu-Au-Mo deposit, Uzbekistan (subduction-related; Pašava et al., 2010); and the Skouries Cu-Au deposit, Greece (post-subduction; this study, Eliopoulos and Economou-Eliopoulos, 1991).

Whole-rock Au, Pd, and Pt concentrations do not show a systematic difference between subduction-related and post-

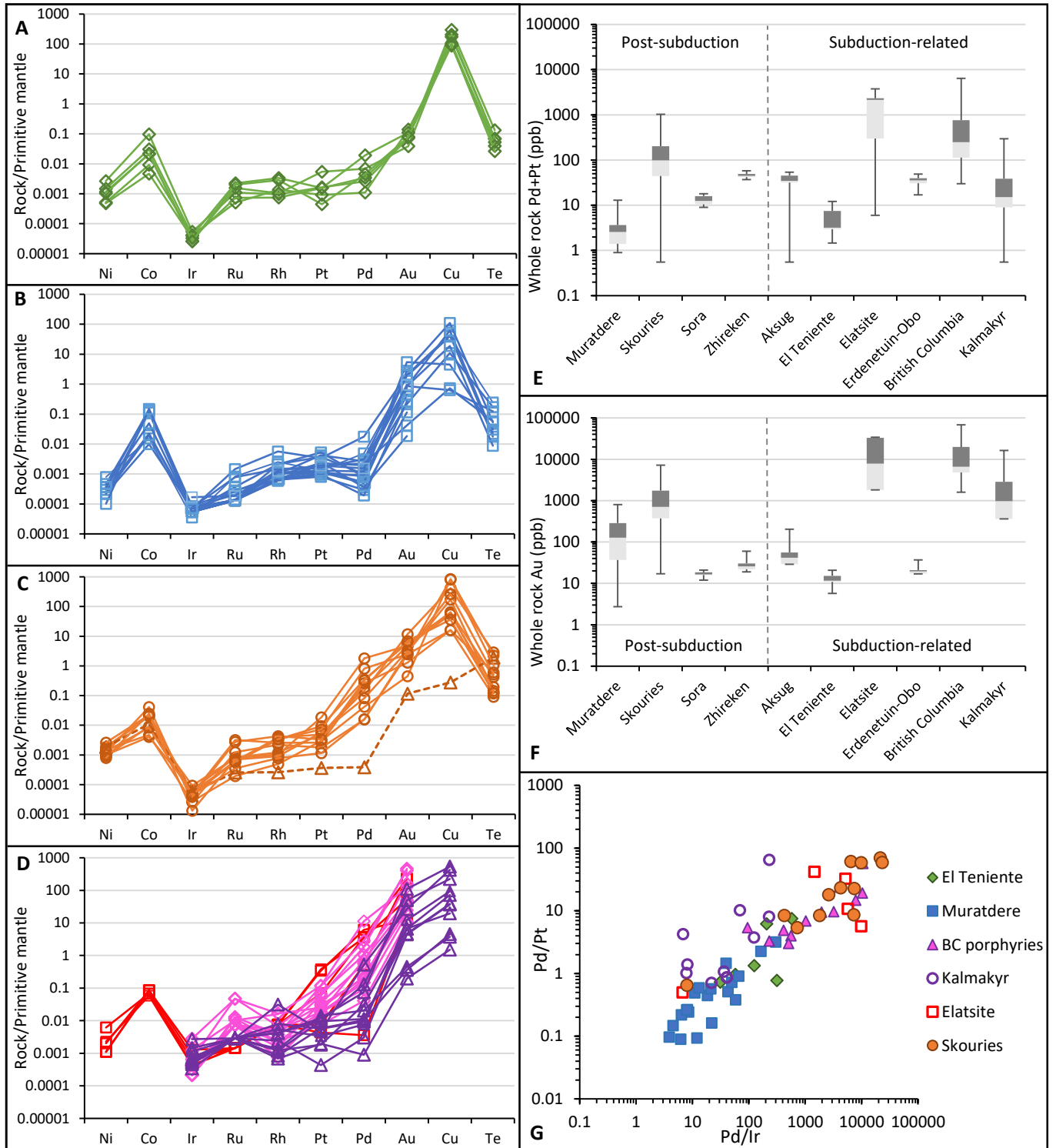


Fig. 8. A-D. Mantle-normalized whole-rock chalcophile and siderophile element profiles for (A) El Teniente. (B) Muratdere. (C) Skouries data from this study, with the dotted line representing the disseminated sulfide sample. (D) Global PGE-enriched porphyry Cu deposit values from Elatsite (red squares: Auge et al., 2005), British Columbia porphyry deposits (pink diamonds: Thompson et al., 2001), and Kalmakyr (purple triangles: Pasava et al., 2010). (E) Logarithmic box and whisker plots, showing the whole-rock concentration of Au from the porphyry deposits above. (F) Logarithmic box and whisker plots, showing the combined whole-rock concentration Pd and Pt from the porphyry deposits above. The box represents the range between the 1st and 3rd quartile, with the darker shaded upper portion indicating the range between the median and the 3rd quartile and whiskers represent range between minimum and maximum values. The dotted line represents the divide between postsubduction and subduction-related deposits. (G) Biplot showing the relationship between Pd/Pt and Pd/Ir in the porphyry deposits above.

subduction deposits (Fig. 8E-F). The Elatsite, Kalmakyr, and British Columbia porphyry deposits contain the highest Au concentrations and these are all subduction-related (Thompson et al., 2001; Augé et al., 2005; Pašava et al., 2010; Fig. 8F), and PGE-rich porphyry deposits are found in both subduction-related and postsubduction settings, as are PGE-poor porphyry deposits (Fig. 8F). This is supported by reports of Au-poor postsubduction deposits, such as the Cu-Mo deposits in the Gangdese belt, Tibet (e.g., Hou et al., 2009) and the Au-poor porphyry Cu deposits in Iran (e.g., Shafiei and Shahbapour, 2008), and suggests that tectonic setting is not the main control on the Au enrichment of porphyry Cu deposits, or on the enrichment of PGE.

*What controls chalcophile and siderophile element concentrations in porphyry Cu deposit source magmas?*

Whole rock chalcophile and siderophile element data normalized to primitive mantle (Palme and O'Neill, 2013) were plotted with elements ordered in decreasing compatibility with minerals that form early from a melt (e.g., Olivine, Cr-spinel, Ni-Fe sulfides; Holwell et al., 2019) in order to compare fractionation patterns between the three deposits from this study (Fig. 8 A-C) and other porphyry Cu deposit ore samples (Fig. 8D). All these systems show the same basic element pattern—a steep fractionation profile with a downturn at Te (Fig. 8A-D). The deposits all have a positive Co anomaly, which is a subduction signature (Hughes et al., 2016), followed by a PGE fractionation curve, with higher levels of PPGE (Pd, Pt, Rh) than IPGE (Ir, Ru, Os). They then peak at Au and Cu, before returning to below mantle values for Te (although Te values were only available for the deposits analyzed during this study; Fig. 8A-C). The Co anomaly is likely present in postsubduction porphyry deposits due to the presence of subduction-modified source material in the subcontinental lithospheric mantle, including residual sulfides from subduction, which would have inherited some geochemical subduction signature (Hughes et al., 2016; Holwell et al., 2019). It is worth noting that this element pattern is also similar to that observed from PGE analysis of unmineralized magma associated with porphyry Cu deposits (Cocker et al., 2015; Hao et al., 2017, 2019; Park et al., 2019).

The biggest difference between deposits is in the relative amounts of Au, Pd, and Te, with Au/Co and Pd/Ir providing the best discriminators (Fig. 4E) between deposits by illustrating the varying amounts of fractionation in chalcophile and siderophile elements. Au/Co, Pd/Pt, and Pd/Ir are higher in Skouries than in both El Teniente and Muratdere (Fig. 4E-F), illustrating the relative enrichment in Pd and Au. Similarly, on a Pt + Pd versus Te + Bi graph, El Teniente and Muratdere plot in the same area, while Skouries contains more of both (Fig. 4D). Given that both Skouries and Muratdere are postsubduction porphyry deposits suggests that tectonic setting is not the control here.

There is a systematic difference in Pd/Pt and Pd/Ir between PGE-enriched and -poor porphyry deposits—Elatsite, Skouries, Kalmakyr, and the British Columbia deposits are PGE-enriched and have higher Pd/Pt and Pd/Ir than the PGE-poor Muratdere and El Teniente deposits (Fig. 8G). However, the main difference between PGE-enriched and -poor porphyry deposits seems to be the overall concentra-

tions of all chalcophile and siderophile elements, rather than any specific fractionation, with many PGE-poor porphyry deposits still containing a relative Pd enrichment over the other PGE (Fig. 8). This enrichment of Pd over Pt may be due to the crystallization of Pt-bearing alloys (Park et al., 2013) and Cr-spinels (Kamenetsky et al., 2015) early in the fractionation history of the source magma. These phases would preferentially take up Pt and IPGE during sulfide-undersaturated fractional crystallization, leaving a source magma with high Pd/Pt and Pd/Ir (Park et al., 2016). Highly oxidized magmas with shallow magma differentiation depth (20–30 km) may not experience sulfide saturation until ore fluid exsolution has occurred in a shallow magma chamber, resulting in a Pd-rich fractionated source magma due to the incompatible behavior of Pd when compared to the more compatible Pt (Park et al., 2016, 2019).

Alternatively, or additionally, the Pd enrichment may be due to a preferential enrichment of Pd over Pt in ore-forming fluids. Several experimental studies have found Pd to have relatively high mobility in high-temperature (>350°C), chloride-rich, oxidized fluids, such as those preserved as metal-bearing fluid inclusions associated with hypogene mineralization in PGE-rich porphyry Cu deposits (Wood and Mountain, 1991; Xiong and Wood, 2000; Augé et al., 2005; Kovalenker et al., 2008; Stefanova et al., 2014; McFall, 2016). This is supported by the low Pd concentration in the disseminated sulfide sample from the Skouries deposit, which does not show the Pd enrichment seen in samples that contain hydrothermal vein mineralization (Fig. 8C). Some studies suggest Pt is relatively immobile in similar fluid conditions (e.g., Scholten et al., 2018). However, studies on condensates from low-density, sulfur-rich magmatic volatiles at arc volcanoes, suggested to be analogous to volatiles exsolved from porphyry deposit source magmas, show that Pt has a higher partition coefficient in those volatiles than Pd (Park et al., 2016, and references therein).

Given the tendency of Au, PGE, and Te to partition into residual sulfides in subduction zones in order to provide metals for an Au (and potentially PGE, Te, and Bi)-enriched subduction-related porphyry Cu deposit, either the formation of residual sulfides must be repressed or the residual sulfides must be transported into the upper crust. If the magma in subduction zones is oxidized then most sulfur would be present as SO<sub>2</sub>, rather than as sulfides (Alt et al., 1993). This would potentially allow chalcophile and siderophile elements, such as Cu and Au, to remain dissolved in the silicate melt, rather than being lost to solid sulfides or sulfide melt (e.g., Wilkinson, 2013). If magma differentiation occurs at shallow depths (<20–30 km) and remains highly oxidized until the exsolution of ore-forming fluids, then any PGE, particularly Pd, may also remain in the silicate melt, as has been suggested for the Cadia and Northparkes magmas (Hao et al., 2017; Lowczak et al., 2018; Park et al., 2019). However, this depends on the  $f_{O_2}$ , pressure, and temperature of the magma, and recent studies suggest that most arc magmas are likely to reach sulfide saturation on ascent (Jugo, 2009; Matjuschkin et al., 2016).

If Au is partitioned into residual sulfides during subduction then the dense sulfides need to be mobilized along with the source melt in order to form an Au-enriched subduction-related deposit, for example, by attraction to low-density volatile

bubbles (Blanks et al., 2020). Any entrained sulfides would likely redissolve with ascent as sulfide solubility increases in a silicate melt with decreasing pressure (Mavrogenes and O'Neill, 1999; Kerr and Leitch, 2005), and Au could then be incorporated into a volatile phase during volatile release (Wilkinson, 2013; Mungall and Brenan, 2014; Holwell et al., 2019). Any remnant, entrained sulfides could also interact with fluids, transferring metals (Mungall et al., 2015). If, however, these sulfides are not transported to the upper crust then subduction-related porphyry deposits may be Cu rich and relatively Au (and other chalcophile and siderophile element) poor (Richards, 2009).

Similarly, Au-rich postsubduction deposits that source their metals from the melting of subduction-modified sulfide-bearing hydrous cumulates in the subcontinental lithosphere need a mechanism to either melt or transport these sulfides. If the magma has a high  $f_{O_2}$  then the sulfides may be remelted, enriching the silicate melt in metal and sulfur (Fiorentini et al., 2018). Alternatively, these sulfides may be transported upward without melting by association with volatiles phases such as mantle-derived carbon in a manner analogous to froth flotation (Blanks et al., 2020).

Thus it is likely that the Au content of the lower crustal source magma for a porphyry Cu deposit is controlled by the oxidation state of the melt (e.g., Sun et al., 2004; Richards, 2015) and/or the presence of volatiles to allow sulfide transport as the source magma rises from the lower crust (e.g., Blanks et al., 2020), regardless of the tectonic setting.

Platinum group elements have higher  $D^{sul/sil}$  than Au and Te (~300,000–500,000 cf. ~10,000; Mungall and Brenan, 2014; Brenan, 2015) and so are likely to remain in any sulfide melt left behind during ascent or after the majority of sulfides are redissolved on ascent (Holwell et al., 2019). In order to form a PGE-enriched porphyry deposit, therefore, either the source magma must remain sulfide undersaturated at all stages up to ore fluid exsolution (Park et al. 2016) or an additional mechanism is needed. Telluride and bismuthide melts have been suggested to perform an important role in Pt and Pd concentration and transport in the source magma of postsubduction porphyry deposits (Helmy et al., 2007; Holwell and McDonald, 2010; McFall et al., 2018; Holwell et al., 2019; Helmy and Botcharnikov, 2020). In magmatic sulfide deposits a Te-rich semimetal melt, in which Pd and Pt are strongly compatible, commonly forms at around 900°C (Helmy et al., 2013; Helmy and Botcharnikov, 2020). This semimetal melt is incompatible with crystalline sulfide (Holwell and McDonald, 2010) and so while sulfide dissolution may occur during the ascent of postsubduction porphyry source magma, enriching the silicate melt in Cu, S, Fe, and possibly Au, if sufficient Te and Bi are present there may also be a coexisting Pd-Pt semimetal melt, which is stable down to temperatures of ~400°C (Ciobanu et al., 2005). This semimetal melt could transport Pd and Pt during ascent—tellurides have been shown to show the same affinity to low-density volatile bubbles as sulfide droplets (Blanks et al., 2020)—and could further concentrate Pd and Pt as any Pd and Pt dissolved in the silicate melt would preferentially partition into a semimetal melt (Helmy et al., 2020). This PGE semimetal melt could be incorporated into volatiles as ligands (Helmy and Botcharnikov, 2020), or poten-

tially entrained as melt droplets (Ciobanu et al., 2005; McFall et al., 2018), during volatile release in the mid to upper crust. Ore-forming fluids in PGE-enriched porphyry Cu deposits, such as Skouries and Elatsite, are Bi enriched (Tarkian et al., 2003; McFall, 2016), and the majority of porphyry-hosted PGM are Bi-Te minerals (e.g., McFall et al., 2018).

This process is unlikely to be limited to postsubduction deposits. Indeed, the PGE-enriched Elatsite deposit is subduction related, as are the PGE-enriched Kalmakyr and British Columbia porphyry deposits (Thompson et al., 2001; Ciobanu et al., 2002; Lips et al., 2004; Augé et al., 2005; von Quadt et al., 2005; Pašava et al., 2010; Gallhofer et al., 2015; Cheng et al., 2018; Menant et al., 2018; Fig. 8F). The mantle wedge is relatively Te-rich (Hattori et al., 2002), as both Te and Bi are present in hydrothermal sulfides in the upper oceanic crust (e.g., Maslennikov et al., 2013; Keith et al., 2017; Martin et al., 2019), with Te also significantly enriched in seafloor sediments and nodules (Lusty et al., 2018). In the oxidized mantle wedge, Te can partition into metasomatic fluids and melts (Brugger et al., 2012; Grundler et al., 2013), as well as into any residual sulfides that provide a potential Te source for postsubduction deposits. It is therefore possible to produce a Te-enriched source magma in both a subduction-related and a postsubduction setting. Any semimetal melt could also segregate and concentrate Au in the same way as Pd and Pt (Ciobanu et al., 2005) and it is notable that while there is no direct correlation between Au and PGE in porphyry Cu deposit samples, perhaps suggesting different depositional mechanisms, PGE-enriched porphyry Cu deposits are always also enriched in Au (Fig. 8E-F).

Ore-forming fluid chemistry will likely also have an effect on the PGE enrichment in porphyry Cu deposits, as for oxidized fluids high temperature and salinity is required to mobilize Pd and Pt (Xiong and Wood, 2000; Hanley et al., 2005; Simon and Pettke, 2009). The PGE-enriched Kalmakyr, Elatsite, and Skouries deposits all have highly saline (>60 wt % NaCl equiv), high-temperature (>500°C), ore-forming fluids (Augé et al., 2005; Kovalenker et al., 2008; Stefanova et al., 2014; McFall, 2016) and this may be another factor. However, the source magma must also be enriched in PGE and the presence of elevated concentrations of Te and Bi may play an important role.

## Conclusions

1. Porphyry Cu deposits can contain potentially economic concentrations of precious metals Au, Ag, Pd, and Pt; and critical metals Te, Se, and Bi. Selenium, and to a certain extent Ag and Bi, are hosted in sulfides. Bornite preferentially hosts Ag and Bi, while Se is present in all sulfides, with higher concentrations in Cu-bearing sulfides. Gold, Pd, Pt, and Te are not present in high concentrations in sulfide minerals and are predominantly hosted in accessory minerals such as electrum, hessite, native Au, and platinum group minerals.
2. Sulfides in postsubduction porphyry Cu deposits are significantly enriched in Bi, Sb, Te, and Se when compared to sulfide minerals from subduction-related deposits, which are significantly enriched in Co and Ag. Care should be taken over drawing comparisons between sulfides,

however, due to their trace element heterogeneity and the presence of precious and critical metal-bearing accessory minerals.

3. Whole-rock analysis shows the postsubduction Muratdere and Skouries deposits contain significantly more Au than the subduction-related El Teniente deposit, with Skouries containing significantly higher concentrations of Pd, Pt, Te, and Bi than both Muratdere and El Teniente. However, comparison with data from literature shows that Au- and PGE-enriched porphyry Cu deposits are formed in both subduction-related and postsubduction tectonic environments, suggesting that enrichment in these elements is independent of coarse tectono-magmatic control.
4. It is therefore likely that the controls on precious and critical metal endowment in porphyry Cu deposit source magmas are the  $f_{O_2}$  of the magma and the presence of volatiles to transport residual sulfides from the lower crust. These sulfides redissolve as the magma ascends, providing a metal-rich source magma. The presence of semimetals such as Te and Bi may facilitate the enrichment of PGE in porphyry Cu deposits by forming a semimetal melt to transport and concentrate Pd and Pt, which would otherwise have remained in any residual sulfides in the lower to mid crust, allowing their incorporation into volatiles during the volatile release stage.

### Acknowledgments

We would like to acknowledge Eldorado Gold Corporation, Tim Baker, and the team at the Skouries site for logistic support in collecting the Skouries samples; Bahri Yildiz and the rest of the Stratex International team in Turkey for logistic support in collecting the Muratdere samples; Simon Kocher for providing access to the Natural History Museum ores collection; and Edward Spencer and Victoria Vry for collecting the samples from El Teniente. We would also like to acknowledge the helpful comments of Jung-Woo Park and one anonymous reviewer. This work was supported by NERC grants NE/M010848/1 "TeaSe: tellurium and selenium cycling and supply" and NE/P017312/1 "From arc magmas to ores (FAMOS): A mineral systems approach."

### REFERENCES

- Abraitis, P.K., Patrick, R.A.D., and Vaughan, D.J., 2004, Variations in the compositional, textural and electrical properties of natural pyrite: A review: *International Journal of Mineral Processing*, v. 74, p. 41–59.
- Alt, J.C., Shanks III, W.C., and Jackson, M.C., 1993, Cycling of sulfur in subduction zones: The geochemistry of sulfur in the Mariana island arc and back-arc trough: *Earth and Planetary Science Letters*, v. 119, p. 477–494.
- Altunkaynak, Ş., and Dilek, Y., 2006, Timing and nature of postcollisional volcanism in western Anatolia and geodynamic implications: *Geological Society of America Special Paper* 409, p. 321–351.
- Ataman, G., 1972, L'age radiométrique du massif granodioritique d'Orhaneli: *Bulletin of the Geological Society of Turkey*, v. 15, p. 125–130.
- Augé, T., Petrunov, R., and Bailly, L., 2005, On the origin of the PGE mineralization in the elatsite porphyry Cu-Au deposit, Bulgaria: Comparison with the Baula-Nuasahi Complex, India, and other alkaline PGE-rich porphyries: *Canadian Mineralogist*, v. 43, p. 1355–1372.
- Blanks, D.E., Holwell, D.A., Fiorentini, M.L., Moroni, M., Giuliani, A., Tassara, S., González-Jiménez, J.M., Boyce, A.J., and Ferrari, E., 2020, Fluxing of mantle carbon as a physical agent for metallogenic fertilization of the crust: *Nature Communications*, v. 11, p. 1–11.
- Bogdanov, K., Filipov, A., and Kehayov, R., 2005, Au-Ag-Te-Se minerals in the Elatsite porphyry-copper deposit, Bulgaria: *Geochemistry, Mineralogy and Petrology*, v. 43, p. 14–19.
- Brenan, J.M., 2015, Se-Te fractionation by sulfide-silicate melt partitioning: Implications for the composition of mantle-derived magmas and their melting residues: *Earth and Planetary Science Letters*, v. 422, p. 45–57.
- Brugger, J., Etschmann, B.E., Grundler, P. V., Liu, W., Testemale, D., and Pring, A., 2012, XAS evidence for the stability of polytellurides in hydrothermal fluids up to 599°C, 800 bars: *American Mineralogist*, v. 97, p. 1519–1522.
- Brun, J.P., and Sokoutis, D., 2007, Kinematics of the southern Rhodope Core Complex (North Greece): *International Journal of Earth Sciences*, v. 96, p. 1079–1099.
- Campbell, I.H., and Naldrett, A.J., 1979, The influence of silicate:sulfide ratios on the geochemistry of magmatic sulfides: *Economic Geology*, v. 74, p. 1503–1506.
- Camus, F., 1975, Geology of the El Teniente orebody with emphasis on wall-rock alteration: *Economic Geology*, v. 70, p. 1341–1372.
- 2002, The Andean porphyry systems: Giant ore deposits: Characteristics, genesis and exploration: *Center for Ore Deposit and Exploration Studies (CODES) Special Publication* 4, p. 5–22.
- Cannell, J., Cooke, D.R., Walshe, J.L., and Stein, H., 2005, Geology mineralization, alteration, and structural evolution of the El Teniente porphyry Cu-Mo deposit: *Economic Geology*, v. 100, p. 979–1003.
- Cheng, Z., Zhang, Z., Chai, F., Hou, T., Santosh, M., Turesebekov, A., and Nurtaev, B.S., 2018, Carboniferous porphyry Cu-Au deposits in the Almalyk orefield, Uzbekistan: the Sarychoku and Kalmakyr examples: *International Geology Review*, v. 60, p. 1–20.
- Chouinard, A., Paquette, J., and Williams-Jones, A.E., 2005, Crystallographic controls on trace-element incorporation in auriferous pyrite from the Pascua epithermal high-sulfidation deposit, Chile-Argentina: *Canadian Mineralogist*, v. 43, p. 951–963.
- Ciobanu, C.L., Cook, N.J., and Stein, H., 2002, Regional setting and geochronology of the Late Cretaceous Banatitic magmatic and metallogenic belt: *Mineralium Deposita*, v. 37, p. 541–567.
- Ciobanu, C.L., Cook, N.J., and Pring, A., 2005, Bismuth tellurides as gold scavengers: *Mineral Deposit Research, Meeting the Global Challenge*: Berlin, Heidelberg, Springer, p. 1383–1386.
- Ciobanu, C.L., Cook, N.J., Kelson, C.R., Guerin, R., Kalleske, N., and Danyushevsky, L., 2013, Trace element heterogeneity in molybdenite fingerprints stages of mineralization: *Chemical Geology*, v. 347, p. 175–189.
- Cocker, H.A., Valente, D.L., Park, J.W., and Campbell, I.H., 2015, Using platinum group elements to identify sulfide saturation in a porphyry Cu system: The El Abra porphyry Cu deposit, northern Chile: *Journal of Petrology*, v. 56, p. 2491–2514.
- Cockerton, A.B.D., and Tomkins, A.G., 2012, Insights into the liquid bismuth collector model through analysis of the Bi-Au Stormont skarn prospect, Northwest Tasmania: *Economic Geology*, v. 107, p. 667–682.
- Cook, N.J., Ciobanu, C.L., Danyushevsky, L.V., and Gilbert, S., 2011, Minor and trace elements in bornite and associated Cu-(Fe)-sulfides: A LA-ICP-MS study: *Geochimica et Cosmochimica Acta*, v. 75, p. 6473–6496.
- Cooke, D.R., Hollings, P., and Walshe, J.L., 2005, Giant porphyry deposits: Characteristics, distribution, and tectonic controls: *Economic Geology*, v. 100, p. 801–818.
- Deditius, A.P., Reich, M., Kesler, S.E., Utsunomiya, S., Chryssoulis, S.L., Walshe, J., and Ewing, R.C., 2014, The coupled geochemistry of Au and As in pyrite from hydrothermal ore deposits: *Geochimica et Cosmochimica Acta*, v. 140, p. 644–670.
- Delaloye, M., and Bingöl, E., 2000, Granitoids from western and northwestern Anatolia: Geochemistry and modeling of geodynamic evolution: *International Geology Review*, v. 42, p. 241–268.
- Eldorado Gold Corporation, 2019, Eldorado gold mineral reserves as of September 30, 2019: (<https://www.eldoradogold.com/assets/resources-and-reserves/default.aspx>).
- Eliopoulos, D.G., and Economou-Eliopoulos, M., 1991, Platinum-group element and gold contents in the Skouries porphyry copper deposit, Chalkidiki Peninsula, northern Greece: *Economic Geology*, v. 86, p. 740–749.
- Fiorentini, M.L., LaFlamme, C., Denyszyn, S., Mole, D., Maas, R., Locmelis, M., Caruso, S., and Bui, T.-H., 2018, Post-collisional alkaline magmatism as gateway for metal and sulfur enrichment of the continental lower crust: *Geochimica et Cosmochimica Acta*, v. 223, p. 175–197.
- Frei, R., 1995, Evolution of mineralizing fluid in the porphyry copper system of the Skouries deposit, northeast Chalkidiki (Greece): Evidence from combined Pb-Sr and stable isotope data: *Economic Geology*, v. 90, p. 746–762.
- Gallhofer, D., Quadt, A.Von, Peytcheva, I., Schmid, S.M., and Heinrich, C.A., 2015, Tectonic, magmatic, and metallogenic evolution of the Late




- Cretaceous arc in the Carpathian-Balkan orogen: *Tectonics*, v. 34, p. 1813–1836.
- George, L., Cook, N.J., Cristiana, C., and Wade, B.P., 2015, Trace and minor elements in galena: A reconnaissance LA-ICP-MS study: *American Mineralogist*, v. 100, p. 548–569.
- George, L.L., Cook, N.J., and Ciobanu, C.L., 2016, Partitioning of trace elements in co-crystallized sphalerite-galena-chalcopyrite hydrothermal ores: *Ore Geology Reviews*, v. 77, p. 97–116.
- George, L.L., Cook, N.J., Crowe, B.B.P., and Ciobanu, C.L., 2018, Trace elements in hydrothermal chalcopyrite: *Mineralogical Magazine*, v. 82, p. 59–88.
- Grundler, P.V., Brugger, J.J., Etschmann, B.E., Helm, L., Liu, W., Spry, P.G., Tian, Y., Testemale, D., and Pring, A., 2013, Speciation of aqueous tellurium (IV) in hydrothermal solutions and vapors, and the role of oxidized tellurium species in Te transport and gold deposition: *Geochimica et Cosmochimica Acta*, v. 120, p. 298–325.
- Gunn, G., 2014, *Critical metals handbook*: John Wiley and Sons, 439 p.
- Hahn, A., 2015, Nature, timing and geodynamic context of polymetallic mineralisation in the Kassandra mining district, North Greece: Ph.D. dissertation, UK, Kingston University.
- Hanley, J.J., Pettke, T., Mungall, J.E., and Spooner, E.T.C.C., 2005, The solubility of platinum and gold in NaCl brines at 1.5 kbar, 600 to 800°C: A laser ablation ICP-MS pilot study of synthetic fluid inclusions: *Geochimica et Cosmochimica Acta*, v. 69, p. 2593–2611.
- Hao, H., Campbell, I.H., Park, J.W., and Cooke, D.R., 2017, Platinum-group element geochemistry used to determine Cu and Au fertility in the Northparkes igneous suites, New South Wales, Australia: *Geochimica et Cosmochimica Acta*, v. 216, p. 372–392.
- Hao, H., Campbell, I.H., Richards, J.P., Nakamura, E., and Sakaguchi, C., 2019, Platinum-group element geochemistry of the Escondida igneous suites, northern Chile: Implications for ore formation: *Journal of Petrology*, v. 60, p. 487–513.
- Hattori, K.H., Arai, S., and Clarke Barrie, D.B., 2002, Selenium, tellurium, arsenic and antimony contents of primary mantle sulfides: *Canadian Mineralogist*, v. 40, p. 637–650.
- Hein, J.R., Koschinsky, A., and Halliday, A.N., 2003, Global occurrence of tellurium-rich ferromanganese crusts and a model for the enrichment of tellurium: *Geochimica et Cosmochimica Acta*, v. 67, p. 1117–1127.
- Helmy, H.M., and Botcharnikov, R., 2020, Experimental determination of the phase relations of Pt and Pd antimonides and bismuthinides in the Fe-Ni-Cu sulfide systems between 1100 and 700°C: *American Mineralogist: Journal of Earth and Planetary Materials*, v. 105, p. 344–352.
- Helmy, H.M., Ballhaus, C., Berndt, J., Bockrath, C., and Wohlgemuth-Uebwasser, C., 2007, Formation of Pt, Pd and Ni tellurides: Experiments in sulfide-telluride systems: *Contributions to Mineralogy and Petrology*, v. 153, p. 577–591.
- Helmy, H.M., Ballhaus, C., Fonseca, R.O.C., and Nagel, T.J., 2013, Fractionation of platinum, palladium, nickel, and copper in sulfide-arsenide systems at magmatic temperature: *Contributions to Mineralogy and Petrology*, v. 166, p. 1725–1737.
- Helmy, H.M., Ballhaus, C., Fonseca, R.O.C., and Leitzke, F.P., 2020, Concentrations of Pt, Pd, S, As, Se and Te in silicate melts at sulfide, arsenide, selenide and telluride saturation: Evidence of PGE complexing in silicate melts?: *Contributions to Mineralogy and Petrology*, v. 175, p. 1–14.
- Holwell, D.A., and McDonald, I., 2010, A review of the behaviour of platinum group elements within natural magmatic sulfide ore systems: *Platinum Metals Review*, v. 54, p. 26–36.
- Holwell, D.A., Fiorentini, M., McDonald, I., Lu, Y., Giuliani, A., Smith, D.J., Keith, M., and Locmelis, M., 2019, A metasomatized lithospheric mantle control on the metallogenic signature of post-subduction magmatism: *Nature Communications*, v. 10, p. 1–10.
- Hou, Z., Yang, Z., Qu, X., Meng, X., Li, Z., Beaudoin, G., et al., 2009, The Miocene Gangdese porphyry copper belt generated during post-collisional extension in the Tibetan orogen: *Ore Geology Reviews*, v. 36(1–3), p. 25–51.
- Hou, Z., Yang, Z., Lu, Y., Kemp, A., Zheng, Y., Li, Q., Tang, J., Yang, Z., and Duan, L., 2015, A genetic linkage between subduction- and collision-related porphyry Cu deposits in continental collision zones: *Geology*, v. 43, p. 247–250.
- Huber, H., Koerber, C., McDonald, I., and Reimold, W.U., 2001, Geochemistry and petrology of Witwatersrand and Dwyka diamictites from South Africa: Search for an extraterrestrial component: *Geochimica et Cosmochimica Acta*, v. 65, p. 2007–2016.
- Hughes, H.S.R., McDonald, I., Faithfull, J.W., Upton, B.G.J., and Loocke, M., 2016, Cobalt and precious metals in sulphides of peridotite xenoliths and inferences concerning their distribution according to geodynamic environment: A case study from the Scottish lithospheric mantle: *Lithos*, v. 240–243, p. 202–227.
- Jenner, F.E., 2017, Cumulate causes for the low contents of sulfide-loving elements in the continental crust: *Nature Geoscience*, v. 10, p. 524–529.
- Jugo, P.J., 2009, Sulfur content at sulfide saturation in oxidized magmas: *Geology*, v. 37, p. 415–418.
- Kamenetsky, V.S., Park, J.-W., Mungall, J.E., Pushkarev, E.V., Ivanov, A.V., Kamenetsky, M.B., and Yaxley, G.M., 2015, Crystallization of platinum-group minerals from silicate melts: Evidence from Cr-spinel-hosted inclusions in volcanic rocks: *Geology*, v. 43, p. 903–906.
- Keith, M., Smith, D.J., Jenkin, G.R.T., Holwell, D.A., and Dye, M.D., 2017a, A review of Te and Se systematics in hydrothermal pyrite from precious metal deposits: Insights into ore-forming processes: *Ore Geology Reviews*, p. 1–14.
- Keith, M., Haase, K.M., Klemd, R., Schwarz-Schampera, U., and Franke, H., 2017b, Systematic variations in magmatic sulphide chemistry from mid-ocean ridges, back-arc basins and island arcs: *Chemical Geology*, v. 451, p. 67–77.
- Kerr, A., and Leitch, A.M., 2005, Self-destructive sulfide segregation systems and the formation of high-grade magmatic ore deposits: *Economic Geology*, v. 100, p. 311–332.
- Kesler, S.E., Chryssoulis, S.L., and Simon, G., 2002, Gold in porphyry copper deposits: Its abundance and fate: *Ore Geology Reviews*, v. 21, p. 103–124.
- Klemm, L.M., Pettke, T., Heinrich, C.A., and Campos, E., 2007, Hydrothermal evolution of the El Teniente deposit, Chile: Porphyry Cu-Mo ore deposition from low-salinity magmatic fluids: *Economic Geology*, v. 102, p. 1021–1045.
- Kuşcu, İ., Tosdal, R.M., Gencalioglu-Kuşcu, G., Friedman, R., and Ullrich, T.D., 2013, Late Cretaceous to middle Eocene magmatism and metallogeny of a portion of the southeastern Anatolian orogenic belt, east-central Turkey: *Economic Geology*, v. 108, p. 641–666.
- Kovalenker, V., Chernyshev, I., Plotinskaya, O., Prokofiev, V., and Koneev, R., 2008, The super-large Kurama porphyry-epithermal gold province (Middle Tien Shan): Key deposits, magmatic and hydrothermal activity age, mineralogical and fluid regime features [abs.]: *International Geological Congress 33, Oslo, Norway, Abstracts, CD-ROM, X-CD Technologies, MRD10*.
- Kroll, T., Muller, D., Seifert, T., Herzig, P. M., and Schneider, A., 2002, Petrology and geochemistry of the shoshonite-hosted Skouries porphyry Cu-Au deposit, Chalkidiki, Greece: *Mineralium Deposita*, v. 37, p. 137–144.
- Kuscü, I., 2016, Magmatic evolution and metallogeny of Turkey [abs.]: *Society of Economic Geologists Conference 2016, Tethyan Tectonics and Metallogeny, Cesme, Turkey, September 25–28, 2016, Abstracts, 2 p*.
- Liégeois, J.-P., Navez, J., Hertogen, J., and Black, R., 1998, Contrasting origin of post-collisional high-K calc-alkaline and shoshonitic versus alkaline and peralkaline granitoids: the use of sliding normalization: *Lithos*, v. 45, p. 1–28.
- Lips, A.L.W., Herrington, R.J., Stein, G., Kozelj, D., Popov, K., and Wijbrans, J.R., 2004, Refined timing of porphyry copper formation in the Serbian and Bulgarian portions of the Cretaceous Carpatho-Balkan belt: *Economic Geology*, v. 99, p. 601–609.
- Liu, H., and Chang, L.L.Y., 1994, Phase relations in the system PbS-PbSe-PbTe: *Mineralogical Magazine*, v. 58, p. 567–578.
- Lowczak, J.N., Campbell, I.H., Cocker, H., Park, J.-W., and Cooke, D.R., 2018, Platinum-group element geochemistry of the Forest Reef Volcanics, southeastern Australia: Implications for porphyry Au-Cu mineralisation: *Geochimica et Cosmochimica Acta*, v. 220, p. 385–406.
- Lusty, P.A.J., Hein, J.R., and Josso, P., 2018, Formation and occurrence of ferromanganese crusts: Earth's storehouse for critical metals: *Elements*, v. 14, p. 313–318.
- Marchev, P., Kaiser-Rohrmeier, M., Heinrich, C., Ovtcharova, M., von Quadt, A., and Raicheva, R., 2005, 2: Hydrothermal ore deposits related to post-orogenic extensional magmatism and core complex formation: The Rhodope Massif of Bulgaria and Greece: *Ore Geology Reviews*, v. 27, p. 53–89.
- Martin, A.J., Keith, M., McDonald, I., Haase, K.M., McFall, K.A., Klemd, R., and MacLeod, C.J., 2019, Trace element systematics and ore-forming processes in mafic VMS deposits: Evidence from the Troodos ophiolite, Cyprus: *Ore Geology Reviews*, v. 106, p. 205–225.
- Matjuschkina, V., Blundy, J.D., and Brooker, R.A., 2016, The effect of pressure on sulphur speciation in mid-to deep-crustal arc magmas and implications for the formation of porphyry copper deposits: *Contributions to Mineralogy and Petrology*, v. 171, p. 66.

- Maslennikov, V. V., Maslennikova, S.P., Large, R.R., Danyushevsky, L.V., Herrington, R.J., and Stanley, C.J., 2013, Tellurium-bearing minerals in zoned sulfide chimneys from Cu-Zn massive sulfide deposits of the Urals, Russia: *Mineralogy and Petrology*, v. 107, p. 67–99.
- Mavrogenes, J.A., and O'Neill, H.S.C., 1999, The relative effects of pressure, temperature and oxygen fugacity on the solubility of sulfide in mafic magmas: *Geochimica et Cosmochimica Acta*, v. 63, p. 1173–1180.
- McDonald, I., and Viljoen, K.S., 2006, Platinum-group element geochemistry of mantle eclogites: A reconnaissance study of xenoliths from the Orapa kimberlite, Botswana: *Transactions of the Institutions of Mining and Metallurgy, sec. B, Applied Earth Science*, v. 115, p. 81–93.
- McFall, K.A., 2016, Critical metals in porphyry copper deposits: Ph.D. thesis, Southampton, England, University of Southampton, 239 p.
- McFall, K.A., Naden, J., Roberts, S., Baker, T., Spratt, J., and McDonald, I., 2018, Platinum-group minerals in the Skouries Cu-Au (Pd, Pt, Te) porphyry deposit: *Ore Geology Reviews*, v. 99, p. 344–364.
- McFall, K., Roberts, S., McDonald, I., Boyce, A.J., Naden, J., and Teagle, D., 2019, Rhenium enrichment in the Muratdere Cu-Mo (Au-Re) porphyry deposit, Turkey: Evidence from stable isotope analyses ( $\delta^{34}\text{S}$ ,  $\delta^{18}\text{O}$ ,  $\delta\text{D}$ ) and laser ablation-inductively coupled plasma-mass spectrometry analysis of sulfides: *Economic Geology*, v. 114, p. 1443–1466.
- McInnes, B.I.A., McBride, J.S., Evans, N.J., Lambert, D.D., and Andrew, A.S., 1999, Osmium isotope constraints on ore metal recycling in subduction zones: *Science*, v. 286, p. 512–516.
- Menant, A., Jolivet, L., Tuduri, J., Loiselet, C., Bertrand, G., and Guillou-Frotter, L., 2018, 3D subduction dynamics: A first-order parameter of the transition from copper- to gold-rich deposits in the eastern Mediterranean region: *Ore Geology Reviews*, v. 94, p. 118–135.
- Mungall, J., and Brenan, J., 2014, Partitioning of platinum-group elements and Au between sulfide liquid and basalt and the origins of mantle-crust fractionation of the chalcophile elements: *Geochimica et Cosmochimica Acta*, v. 125, p. 265–289.
- Mungall, J.E., Brenan, J.M., Godel, B., Barnes, S.J., and Gaillard, F., 2015, Transport of metals and sulphur in magmas by flotation of sulphide melt on vapour bubbles: *Nature Geoscience*, v. 8, p. 216–219.
- Palme, H., and O'Neill, H., 2013, Cosmochemical estimates of mantle composition: Elsevier, p. 1–39.
- Park, J.-W., Campbell, I.H., and Arculus, R.J., 2013, Platinum-alloy and sulfur saturation in an arc-related basalt to rhyolite suite: Evidence from the Pual Ridge lavas, the eastern Manus Basin: *Geochimica et Cosmochimica Acta*, v. 101, p. 76–95.
- Park, J.-W., Campbell, I.H., and Kim, J., 2016, Abundances of platinum group elements in native sulfur condensates from the Niutahi-Motutahi submarine volcano, Tonga rear arc: Implications for PGE mineralization in porphyry deposits: *Geochimica et Cosmochimica Acta*, v. 174, p. 236–246.
- Park, J.-W., Campbell, I.H., Malaviarachi, S.P.K., Cocker, H., Hao, H., and Kay, S.M., 2019, Chalcophile element fertility and the formation of porphyry Cu  $\pm$  Au deposits: *Mineralium Deposita*, v. 54, p. 657–670.
- Pašava, J., Vymazalová, A., Košler, J., Koneev, R.I., Jukov, A.V., and Khalmatov, R.A., 2010, Platinum-group elements in ores from the Kalmakyr porphyry Cu-Au-Mo deposit, Uzbekistan: Bulk geochemical and laser ablation ICP-MS data: *Mineralium Deposita*, v. 45, p. 411–418.
- Pašava, J., Svojtka, M., Veselovský, F., Ďurišová, J., Ackerman, L., Pour, O., Drábek, M., Halodová, P., and Haluzová, E., 2016, Laser ablation ICPMS study of trace element chemistry in molybdenite coupled with scanning electron microscopy (SEM)—an important tool for identification of different types of mineralization: *Ore Geology Reviews*, v. 72, p. 874–895.
- Patten, C., Barnes, S.J., Mathez, E.A., and Jenner, F.E., 2013, Partition coefficients of chalcophile elements between sulfide and silicate melts and the early crystallization history of sulfide liquid: LA-ICP-MS analysis of MORB sulfide droplets: *Chemical Geology*, v. 358, p. 170–188.
- Piercey, S.J., 2014, Modern analytical facilities. 2. A review of quality assurance and quality control (QA/QC) procedures for lithochemical data: *Geoscience Canada*, v. 41, p. 75–88.
- Prichard, H.M., Knight, R.D., Fisher, P. C., McDonald, I., Zhou, M.F., and Wang, C.Y., 2013, Distribution of platinum-group elements in magmatic and altered ores in the Jinchuan intrusion, China: An example of selenium remobilization by postmagmatic fluids: *Mineralium Deposita*, v. 48, p. 767–786.
- von Quadt, A., Moritz, R., Peytcheva, I., and Heinrich, C.A., 2005, 3: Geochronology and geodynamics of Late Cretaceous magmatism and Cu-Au mineralization in the Panagyurishte region of the Apuseni-Banat-Timok-Srednogorie belt, Bulgaria: *Ore Geology Reviews*, v. 27, p. 95–126.
- Reich, M., Kesler, S.E., Utsunomiya, S., Palenik, C.S., Chryssoulis, S.L., and Ewing, R.C., 2005, Solubility of gold in arsenian pyrite: *Geochimica et Cosmochimica Acta*, v. 69, p. 2781–2796.
- Richards, J.P., 2009, Postsubduction porphyry Cu-Au and epithermal Au deposits: Products of remelting of subduction-modified lithosphere: *Geology*, v. 37, p. 247–250.
- 2015, The oxidation state, and sulfur and Cu contents of arc magmas: implications for metallogeny: *Lithos*, v. 233, p. 27–45.
- Ringwood, A.E., 1977, Petrogenesis in island arc systems, in Talwani, M., Pitman III, W.C., eds., *Island arcs, deep sea trenches and back-arc basins*, v. 1: American Geological Union, p. 311–324.
- Scholten, L., Watenphul, A., Beermann, O., Testemale, D., Ames, D., and Schmidt, C., 2018, Nickel and platinum in high-temperature  $\text{H}_2\text{O} + \text{HCl}$  fluids: Implications for hydrothermal mobilization: *Geochimica et Cosmochimica Acta*, v. 224, p. 187–199.
- Shafiei, B., and Shahabpour, J., 2008, Gold distribution in porphyry copper deposits of Kerman region, southeastern Iran: *Journal of Sciences Islamic Republic of Iran*, v. 19, p. 247–260.
- Sillitoe, R.H., 1973, The tops and bottoms of porphyry copper deposits: *Economic Geology*, v. 68, p. 799–815.
- 2010, Porphyry copper systems: *Economic Geology*, v. 105, p. 3–41.
- Simon, A.C., and Pettke, T., 2009, Platinum solubility and partitioning in a felsic melt-vapor-brine assemblage: *Geochimica et Cosmochimica Acta*, v. 73, p. 438–454.
- Simon, G., Kesler, S.E., Essene, E.J., and Chryssoulis, S.L., 2000, Gold in porphyry copper deposits: Experimental determination of the distribution of gold in the Cu-Fe-S system at 400° to 700°C: *Economic Geology*, v. 95, p. 259–270.
- Sinclair, W.D., 2007, Porphyry deposits: Geological Association of Canada, Mineral Deposits Division, Special Publication no. 5, p. 223–243.
- Siron, C.R., Thompson, J.F.H., Baker, T., Friedman, R., Tsitsanis, P., Russell, S., Randall, S., and Mortensen, J., 2016, Magmatic and metallogenic framework of Au-Cu porphyry and polymetallic carbonate-hosted replacement deposits of the Kassandra mining district, northern Greece: *Society of Economic Geologists Special Publication 19*, p. 29–55.
- Siron, C.R., Rhys, D., Thompson, J.F.H., Baker, T., Veligrakis, T., Camacho, A., and Dalampiras, L., 2018, Structural controls on porphyry Au-Cu and Au-rich polymetallic carbonate-hosted replacement deposits of the Kassandra mining district, northern Greece: *Economic Geology*, v. 113, p. 309–345.
- Skewes, M.A., and Stern, C.R., 2007, Geology, mineralization, alteration, and structural evolution of the El Teniente porphyry Cu-Mo deposit—a discussion: *Economic Geology*, v. 102, p. 1165–1170.
- Skewes, M.A., Arevalo, A., Floody, R., Zuniga, P. H., and Stern, C., 2002, The giant El Teniente breccia deposit: Hypogene copper distribution and emplacement: *Society of Economic Geologists Special Publication 9*, p. 299–332.
- Spencer, E.T., 2015, The transport and deposition of molybdenum in porphyry ore systems: London, Imperial College London, 301 p.
- Spencer, E.T., Wilkinson, J.J., Creaser, R.A., and Seguel, J., 2015, The distribution and timing of molybdenite mineralization at the El Teniente Cu-Mo porphyry deposit, Chile: *Economic Geology*, v. 110, p. 387–421.
- Stefanova, E., Driesner, T., Zajacz, Z., Heinrich, C.A., Petrov, P., and Vasilev, Z., 2014, Melt and fluid inclusions in hydrothermal veins: The magmatic to hydrothermal evolution of the Elatsite porphyry Cu-Au deposit, Bulgaria: *Economic Geology*, v. 109, p. 1359–1381.
- Stratex International, 2016, Muratdere JORC compliant resource: Stratex, Annual Report for 2017, 56 p.
- Sugaki, A., Kitakaze, A., and Hayashi, K., 1981, Synthesis of minerals in the Cu-Fe-Bi-S system under hydrothermal condition and their phase relations: *Bulletin de Mineralogie*, v. 104, p. 484–495.
- 1984, Hydrothermal synthesis and phase relations of the polymetallic sulfide system, especially on the Cu-Fe-Bi-S system: *Materials Science of the Earth's Interior*, p. 545–583.
- Sun, W., Arculus, R.J., Kamenetsky, V. S., and Binns, R.A., 2004, Release of gold-bearing fluids in convergent margin magmas prompted by magnetite crystallization: *Nature*, v. 431, p. 975–978.
- Sun, W., Fang Huang, R., Li, H., Bin Hu, Y., Chan Zhang, C., Jun Sun, S., Peng Zhang, L., Ding, X., Ying Li, C., Zartman, R.E., and Xing Ling, M., 2015, Porphyry deposits and oxidized magmas: *Ore Geology Reviews*, v. 65, p. 97–131.
- Tarkian, M., and Stribny, B., 1999, Platinum-group elements in porphyry copper deposits: a reconnaissance study: *Mineralogy and Petrology*, v. 65, p. 161–183.

- Tarkian, M., Hünten, U., Tokmakchieva, M., Bogdanov, K., Hunken, U., Tokmakchieva, M., and Bogdanov, K., 2003, Precious-metal distribution and fluid-inclusion petrography of the Elatsite porphyry copper deposit, Bulgaria: *Mineralium Deposita*, v. 38, p. 261–281.
- Tekeli, O., 1981, Subduction complex of pre-Jurassic age, northern Anatolia, Turkey: *Geology*, v. 9, p. 68–72.
- Thompson, J.F.H., Lang, J.R., and Stanley, C.R., 2001, Platinum group elements in alkaline porphyry deposits, British Columbia: *Exploration and Mining in British Columbia*, v. pt. B, p. 57–64.
- Tooth, B., Brugger, J., Ciobanu, C., and Liu, W., 2008, Modeling of gold scavenging by bismuth melts coexisting with hydrothermal fluids: *Geology*, v. 36, p. 815–818.
- Tooth, B., Ciobanu, C.L., Green, L., O'Neill, B., and Brugger, J., 2011, Bi-melt formation and gold scavenging from hydrothermal fluids: An experimental study: *Geochimica et Cosmochimica Acta*, v. 75, p. 5423–5443.
- Vry, V., 2010, Geological and hydrothermal fluid evolution at El Teniente, Chile: London, Imperial College London.
- Vry, V.H., Wilkinson, J.J., Seguel, J., and Millán, J., 2010, Multistage intrusion, brecciation, and veining at El Teniente, Chile: *Evolution of a nested porphyry system: Economic Geology*, v. 105, p. 119–153.
- Wilkinson, J.J., 2013, Triggers for the formation of porphyry ore deposits in magmatic arcs: *Nature Geoscience*, v. 6, p. 917–925.
- Wood, S.A., and Mountain, B.W., 1991, Hydrothermal solubility of palladium in chloride solutions from 300° to 700°C: Preliminary experimental results—a discussion: *Economic Geology*, v. 86, p. 1562–1563.
- Xiong, Y., and Wood, S.A., 2000, Experimental quantification of hydrothermal solubility of platinum-group elements with special reference to porphyry copper environments: *Mineralogy and Petrology*, v. 68, p. 1–28.

---



**Katie McFall** is a geologist and geochemist who specializes in magmatic and magmatic-hydrothermal mineral deposits. She is currently an economic geology lecturer at University College London, following time as a postdoctoral research associate at Cardiff University, researching the role of volatiles in the formation of magmatic sulfide deposits in layered ultramafic intrusions. Katie received her M.Sci. and Ph.D. (2016) degrees from the University of Southampton, UK. She specializes in ore mineral chemistry and fluid inclusion analysis and has worked on a range of deposit types, applying a wide variety of techniques to understand ore deposit formation and the behavior of chalcophile and critical elements in magmatic-hydrothermal systems.

